A CVID-associated variant in the ciliogenesis protein CCDC28B disrupts immune synapse assembly

Nagaja Capitani
University of Siena
Anna Onnis
University of Siena
FRANCESCA FINETTI
University of Siena https://orcid.org/0000-0002-3421-1637
Chiara Cassioli
University of Siena
Alessandro Plebani
Brescia University Hospital
Jlenia Brunetti
University of Siena https://orcid.org/0000-0001-8144-7186
Arianna Troilo
University of Florence
Sofia D'Elios
University of Pisa
Manuela Baronio
Brescia University Hospital
Luisa Gazzurrelli
Brescia University Hospital
Daniel Billadeau
Mayo Clinic
Mario D'Elios
University of Florence
Vassilios Lougaris
Brescia University Hospital
Cosima Baldari (baldari@unisi.it)
University of Siena https://orcid.org/0000-0002-4414-6744

Article

Keywords: CVID T cells, CCDC28B, C211T allele, Ciliogenesis proteins

Posted Date: October 22nd, 2020

DOI: https://doi.org/10.21203/rs.3.rs-86351/v1

Version of Record: A version of this preprint was published at Cell Death & Differentiation on July 22nd, 2021. See the published version at https://doi.org/10.1038/s41418-021-00837-5.

A CVID-associated variant in the ciliogenesis protein CCDC28B disrupts immune synapse assembly

Nagaja Capitani,[1*] Anna Onnis,[1] Francesca Finetti,[1] Chiara Cassioli,[1] Alessandro Plebani,[2] Jlenia Brunetti,[3] Arianna Troilo,[4] Sofia D'Elios,[5] Manuela Baronio,[2] Luisa Gazzurrelli,[2] Daniel D. Billadeau,[6] Mario Milco D'Elios,[4] Vassilios Lougaris,[2] Cosima T. Baldari[1*]

[1]Department of Life Sciences, University of Siena; [2]Department of Clinical and Experimental Sciences, University of Brescia, and ASST-Spedali Civili of Brescia, Brescia, Italy; [3]Department of Medical Biotechnologies, University of Siena, Siena, Italy; [4]Department of Experimental and Clinical Medicine, University of Florence, Florence, Italy; [5]Department of Clinical and Experimental Medicine, University of Pisa, Pisa, Italy; [6]Division of Oncology Research, Schulze Center for Novel Therapeutics, Mayo Clinic, Rochester, MN, United States.

Running title: A CVID-associated CCDC28B variant impairs IS assembly

Correspondence: Prof. Cosima T Baldari, email baldari@unisi.it; Dr. Nagaja Capitani, email capitani2@unisi.it

ABSTRACT

Ciliogenesis proteins orchestrate vesicular trafficking pathways that regulate immune synapse (IS) assembly in the non-ciliated T cells. We hypothesized that ciliogenesis-related genes might be disease candidates for common variable immunodeficiency with impaired T-cell function (T-CVID). We identified a heterozygous, predicted pathogenic variant in the ciliogenesis protein CCDC28B present with increased frequency in a large CVID cohort. We show that CCDC28B participates in IS assembly by regulating polarized T-cell antigen receptor (TCR) recycling. This involves the CCDC28B-dependent, FAM21-mediated recruitment of the actin regulator WASH to retromer at early endosomes to promote actin polymerization. The CVID-associated CCDC28B^{R25W} variant failed to interact with FAM21, leading to impaired synaptic TCR recycling. CVID T cells carrying the *ccdc28b* C211T allele displayed IS defects mapping to this pathway that were corrected by overexpression of the wild-type allele. These results identify a new disease gene in T-CVID and pinpoint CCDC28B as a new player in IS assembly.

INTRODUCTION

Antibody deficiency, typically related to a clinical history of recurrent infections, is the hallmark of CVID, the most common inheritable immunodeficiency disorder. This common defect is associated with a wide range of highly heterogeneous clinical manifestations that include, beside infections, chronic lung disease, granulomatous disease, autoimmunity, lymphomas and gastrointestinal disease[1]. Based on the heterogeneity in these clinical presentations, CVID has been hypothesized to represent a group of different immune disorders unified by hypogammaglobulinemia. Consistent with this hypothesis, CVID has been associated in a substantial proportion of patients not only with intrinsic defects in B-cell maturation and antibody class switching, but also with defects in T-cell activation and helper function[2]. To date 68 disease genes have been identified in CVID, the majority of which encode proteins directly implicated in B-cell costimulation or immunoglobulin class switching[3,4]. Among the gene products the function of which is not restricted to B cells, of particular interest are ICOS, a costimulatory molecule which plays a key role in helper T cell differentiation[5], the tyrosine kinase Itk[4] and the co-inhibitory receptor CTLA-4[4,6]. We and others have previously reported defects in T-cell antigen receptor (TCR) signaling in CVID patients with impaired T-cell responses (T-CVID)[7-9], which we have circumscribed in a subgroup of patients to a deficiency in the guanine nucleotide exchanger Vav1[10]. In one patient this defect was caused by a sporadic deletion in one Vav1 allele[11], providing proof-of-concept that a genetic lesion in the TCR signaling machinery may underlie CVID.

T-cell activation requires TCR signaling to be topologically orchestrated at the highly organized interface that T cells form upon contact with a cognate antigen presenting cell (APC), known as the immune synapse (IS)[12]. One of the central processes in IS assembly is polarized TCR recycling, which ensures the transport to the IS of endosomal TCRs to sustain signaling[13,14], highlighting vesicular trafficking as a potential new disease process in T-cell related immunodeficiencies. Our unexpected finding that components of the intraflagellar transport (IFT) system that controls ciliogenesis contribute to IS assembly in the non-ciliated T cell by regulating polarized TCR recycling[15] has pinpointed the ciliogenesis machinery as a source of candidate genes. Indeed, we and others have implicated a variety of ciliogenesis regulators in IS assembly and T cell activation[16-18]. Here we have tested the hypothesis that mutations in the genes encoding IFT proteins or other functional components of this system may underlie T-CVID of unknown aetiology. Starting with the identification of an increased frequency in a cohort of 101 CVID patients of a potentially pathogenic SNP in the gene encoding the ciliary protein Coiled-Coil Domain Containing 28B (CCDC28B)[19,20], we addressed the function of CCDC28B in IS assembly. We show that CCDC28B promotes actin polymerization on endosomes carrying recycling TCRs by recruiting the actin regulator WASH and its partner FAM21, thereby allowing for their retrograde traffic to the synaptic membrane. Additionally, we provide evidence that the CVID-associated SNP impairs the ability of CCDC28B to recruit the FAM21-WASH complex to endosomal TCRs and its association with the retromer complex, resulting in their failure to undergo polarized recycling. The data identify a new pathogenic mutation in T-CVID and highlight the ciliary protein CCDC28B as a new player in TCR trafficking and IS assembly.

RESULTS

A pathogenic variant of *ccdc28b* is present with an increased frequency in CVID

To investigate the potential implication of ciliogenesis proteins in the T-cell defects associated with CVID (T-CVID) we carried out a NGS analysis of the coding sequences of the genes encoding ciliary proteins known to participate in cargo sorting and targeting to the cilium and for their intraciliary transport. For the analysis we selected 7 CVID patients classified as T-CVID based on their impaired T-cell proliferative response to an anti-CD3 mAb. High coverage exon sequencing revealed the presence of known or novel predicted pathogenic variants in 5 ciliopathy-related genes in individual patients, all heterozygous (unpublished results).

A large cohort of CVID, comprising 101 patients, was tested by Sanger sequencing for the presence of the variants in the 5 ciliopathy-related genes identified by NGS. These variants were present only in the individual patients initially subjected to exon sequencing with the exception of one, mapping to *ccdc28b* encoding the ciliogenesis protein CCDC28B[19,20], which was found in heterozygosity in 9/101 patients, hence with a frequency of 4.45%. This variant (Ensembl rs1407134) was also present in the healthy population, however with a frequency in the corresponding ethnic group of 2% (based on allele frequencies in the 1000 Genomes Project Phase 3 and the Genome Aggregation database). This variant has a C>T transversion at position 211 of the transcript (NM_024296.5), which results in a R>W substitution at position 25 of the protein (Fig.1A). The increased frequency of this variant in CVID prompted us to investigate the role of CCDC28B in the process of IS assembly, which is coordinated

by ciliary proteins[21], and assess the potential pathogenic outcome of the heterozygous R25W mutation.

CCDC28B is required for IS assembly

CCDC28B is a coiled-coil (CC) domain-containing pericentriolar protein that interacts and colocalizes with the Bardet-Biedl syndrome (BBS) proteins[19] (Fig.1A). CCDC28B has been shown to modulate cilia length both in cultured cells and in vivo in zebrafish[19,20], however the underlying mechanisms remain to be fully elucidated. CCDC28B is expressed in T cells at levels comparable to ciliated cells, as assessed by immunoblot analysis of Jurkat and primary T cells and of the ciliated human hTERT-immortalized fibroblast line (Fig.1B). Co-localization analyses in T cells showed that CCDC28B has a largely centrosomal localization, similar to ciliated cells, as assessed by co-staining for γ-tubulin (Fig.1C,D). Staining for endomembrane markers showed that CCDC28B also co-localizes with early ($Rab5^+$) endosomes and, to a lesser extent, with recycling ($Rab11^+$) endosomes, but not with the Golgi apparatus ($GM130^+$) (Fig.1C,D). Of note, the $CCDC28B^+$ compartment polarized towards the T cell:APC contact together with the centrosome in conjugates formed by Jurkat cells with SEE-loaded Raji cells used as APC (Fig.1E). This result was validated in primary peripheral blood T cells, which were stimulated with Raji cells pulsed with a combination of SEA, SEB and SEE to cover a substantial proportion of the TCR Vβ repertoire and hence maximize the number of responding T cells (Fig.1F).

To address the role of CCDC28B in IS assembly Jurkat T cells were depleted of CCDC28B expression by siRNA-mediated silencing (Fig.S1A). Control and CCDC28B knockdown (KD) Jurkat cells, which expressed similar levels of surface CD3 (Fig.S1B), were compared for their ability to form functional mature immune synapses (15 min conjugation). Three functional readouts were used, namely accumulation of the TCR:CD3 complex and phosphotyrosine signaling at the T cell:APC contact, and centrosome polarization towards the APC. IS defects were observed in CCDC28B KD cells, as assessed by confocal imaging which revealed an impairment in synaptic TCR accumulation (Fig.2A,B). This was paralleled by a reduction in tyrosine phosphoprotein staining in CCDC28B-deficient T cells, indicating a defect in phosphotyrosine signaling at the mature IS (Fig.2A,B), which was confirmed by flow cytometry (Fig.S2A). Similar to the plasma membrane pool, the endosomal TCR pool (eCD3) also failed to polarize towards the IS in cells depleted of CCDC28B (Fig.2A,B; Fig.S2B). At variance, centrosome polarization was not affected (Fig.2A,B; Fig.S2B), indicating that CCDC28B is dispensable for this step. Similar results were obtained when Jurkat cells were depleted of CCDC28B by CRISPR-Cas9 gene editing (Fig. S3A-C; Fig.S1A,B). The results were validated on primary T cells stimulated with SEA/SEB/SEE-pulsed Raji cells (Fig.2C; Fig.S1B,C). The defects observed in CCDC28-deficient T cells were rescued by reconstitution of CCDC28B expression (Fig.2D; Fig.S1D), confirming the implication of this protein in IS assembly.

CCDC28B is required for polarized TCR recycling to the IS

Centrosome translocation to the subsynaptic area is triggered by TCR signaling[12]. The fact that centrosome polarization occurs normally in CCDC28B-deficient T cells (Fig.2A-C) suggests that the initial steps in IS assembly do not require this protein. Consistent with this notion, the initial accumulation at the nascent IS (5 min conjugation) of either the TCR:CD3 complex or tyrosine phosphoproteins was not affected by CCDC28B deficiency (Fig.2A; Fig.S2B). Since TCR signaling is sustained by the endosomal pool that is delivered to the IS by polarized recycling[22], we hypothesized that the defect in synaptic TCR accumulation at the mature IS in CCDC28B-deficient T cells could result from impaired recycling. To test this hypothesis surface TCRs were labelled with an anti-CD3 mAb and incubated at 37°C to allow for internalization of the TCR:mAb complexes. Internalized TCRs were tracked in antigen-specific conjugates using fluorochrome-labelled secondary antibodies. Conjugates were either not permeabilized to visualize the TCRs that had recycled to the plasma membrane, or alternatively permeabilized to detect their intracellular localization.

Confocal imaging of non-permeabilized antigen-specific conjugates showed that internalized antibody-tagged TCRs (tCD3) failed to effectively concentrate at the IS in CCDC28B-deficient Jurkat cells (Fig.3A, upper panel), indicating a defect in polarized recycling. Analysis of permeabilized conjugates showed that endosomes carrying tCD3s remained dispersed away from the T cell:APC contact (Fig.3A, lower panel), suggesting that CCDC28B is required for their translocation to the IS. Similar results were obtained on primary T cells (Fig.3B).

CCDC28B is required for TCR-dependent F-actin polymerization

Endosome recycling is dependent on the concerted action of the actin and tubulin cytoskeletons. Local polymerization of actin filaments on endosomes generates force for scission and coupling of the resulting vesicles to the microtubule minus-end motor dynein for transport towards the centrosome[23,24]. CCDC28B deficiency in zebrafish has been reported to result in actin defects in muscle fibers[20], suggesting that CCDC28B may participate in the pathway that controls actin polymerization in T cells. To test this possibility F-actin was first quantified by flow cytometry in control and CCDC28B KD T cells stimulated with anti-CD3 mAb. Activation-dependent F-actin polymerization was impaired in CCDC28B-deficient T cells (Fig.4A). Additionally, CCDC28B-deficient cells failed to efficiently spread and formed an irregular and broken F-actin ring when plated on coverslips coated with anti-CD3 mAbs, as assessed by total internal reflection fluorescence (TIRF) microscopy (Fig.4B). Consistent with this finding, a significant reduction in F-actin accumulation at the synaptic membrane was observed in the absence of CCDC28B in both Jurkat and primary T cells (Fig.4C,D; Fig.S3D), which could be accounted for by the defect in sustained signaling caused by impaired TCR recycling. These results map CCDC28B to the pathway that couples TCR signaling to actin polymerization.

Interestingly, the ability of F-actin^{+} endosomes to effectively polarize towards the IS was reduced in CCDC28B-deficient Jurkat cells, as assessed by measuring their distance from the synaptic contact (Fig.4E). Co-staining tCD3 with phalloidin in antigen-specific conjugates revealed a reduction in the proportion of endosomes carrying tCD3 that were positive for F-actin in CCDC28B-deficient T cells (Fig.4E). The

co-localization of tCD3 and F-actin on individual endosomes was also reduced in these cells (Fig.4E). These results suggest that the TCR recycling defects observed in CCDC28B-deficient T cells may result from a failure to polymerize new actin filaments on endosomes. Since the endosomal TCR pool is too small for a detailed analysis in freshly purified primary T cells, these results were validated on T cell blasts (generated by peripheral blood mononuclear cell stimulation with SEA/SEB/SEE and supplemented with IL-2 as described in figure S4A), which resulted in a substantial increase in endosome-associated TCRs (Fig.4F; Fig.S4B).

CCDC28B is required for recruitment of the actin regulator WASH and its adaptor FAM21 to retromer-associated TCRs at early endosomes

The actin regulator WASH recruits the actin nucleation factor Arp2/3 on endosomes undergoing retrograde trafficking to promote local F-actin polymerization through its interaction with the adaptor FAM21[25]. WASH$^+$ endosomes failed to polarize towards the IS in CCDC28B-deficient T cells, at variance with control cells (Fig.5A). Additionally, co-staining with phalloidin showed a reduction in the proportion of WASH$^+$ endosomes positive for F-actin$^+$ (Fig.5A and S3E,F; Fig.S5A for primary T cell blasts), suggesting a role for CCDC28B in WASH recruitment to endosomes and the subsequent local F-actin polymerization. Consistent with this notion, imaging tCD3s in antigen-specific conjugates co-stained for WASH showed that the proportion of endosomes carrying tCD3 and positive for WASH was reduced in CCDC28B-deficient T cells (Fig.5B; Fig.S5B). The co-localization of tCD3 and WASH on individual endosomes was also reduced in CCDC28B-deficient T cells (Fig.5B; Fig.S5B for

primary T cell blasts). Similar results were obtained when T cells were co-stained for tCD3 and FAM21 (Fig.5C; Fig.S5C). Hence CCDC28B is required for coupling the FAM21/WASH complex to recycling TCRs to promote local F-actin polymerization for their retrograde transport to the synaptic membrane.

WASH-dependent actin polymerization occurs at early, $Rab5^+$ endosomes (EE), where branched actin provides mechanical force for the abscission of vesicles enriched in receptors destined for recycling[25]. The EE localization of WASH is mediated by FAM21, which interacts with the EE-associated retromer complex[26,27]. We asked whether CCDC28B is implicated in the recruitment of the WASH/FAM21 complex to EEs. A reduction in the co-localization of WASH with Rab5 on individual endosomes was observed in CCDC28B-deficient T cells (Fig.6A). Similar results were obtained for $FAM21^+$ endosomes (Fig.6B), suggesting that CCDC28B regulates the transit of recycling TCRs from EEs to recycling endosomes by contributing to the FAM21-dependent recruitment of WASH to EEs.

To test this hypothesis, we used an immunoprecipitation approach designed to selectively pull down tCD3s to ask whether CCDC28B interacts with recycling TCRs, and to address the outcome of CCDC28B deficiency on the local recruitment of the FAM21/WASH and retromer complexes. Cells were incubated with anti-CD3mAb at 37°C to allow for internalization of antibody-bound TCRs and then acid-stripped to remove antibodies bound to residual TCR complexes. After cell lysis, tCD3:Ab complexes were immunoprecipitated using protein A-Sepharose (Fig.S6A). Immunoblot analysis showed that CCDC28B associates with tCD3s (Fig.6C). Consistent with the fact that the TCR undergoes retromer-mediated sorting with the

assistance of the WASH complex, an association of VPS35 (a core retromer component)[28], FAM21 and WASH with tCD3s was also detected (Fig.6C). The ability of tCD3s to recruit FAM21 and WASH, but not VPS35, was compromised in CCDC28B-deficient T cells (Fig.6C). Hence CCDC28B couples the FAM21/WASH complex to retromer-associated recycling TCRs.

To elucidate the interactions that occur between CCDC28B, WASH/FAM21 and VPS35 we first tested their association with CCDC28B in Jurkat cells transfected with GFP-tagged CCDC28B and subjected to immunoprecipitation with anti-GFP antibodies. VPS35, FAM21 and WASH were found to form a complex with CCDC28B (Fig.6D; Fig.S7A,B for reciprocal immunoprecipitations). CCDC28B deficiency impaired the ability of WASH to interact with VPS35 and FAM21, as assessed by immunoblot of WASH-specific immunoprecipitates (Fig.6E). The association of WASH with its effectors α-tubulin and the Arp2/3 subunit ARPC3 was also compromised in CCDC28B KD T cells (Fig.S7C). Similarly, the ability of VPS35 to interact with WASH and FAM21 was impaired in CCD28B-deficient T cells (Fig.6F)

To confirm these results and map the interactions of CCDC28B on FAM21 and WASH we used a panel of GST-tagged deletion mutants of the latter proteins (Fig.S6B). FAM21 associates with WASH through its N-terminal domain that establishes an interaction with the N-terminal domain of WASH, while it associates with VPS35/retromer at EEs preferentially through multiple L-F-[D/E](3-10)-L-F repeats within its disordered tail (see scheme in figure S5C)[26,29,30]. Pull-down experiments with GSH-Sepharose using GST-tagged constructs encoding the individual N- and C-terminal portions of the repeat-rich tail of FAM21 (FAMn and FAMc, respectively, see

Fig.S6B) revealed that CCDC28B interacts specifically with FAM21c (Fig.6G). As reported[26], this is the FAM21 region also responsible for α-tubulin binding (Fig.S7D). No interaction with WASH was observed (Fig.6G), consistent with the lack of the N-terminal domain of FAM21 where the interaction with WASH has been mapped[26] (Fig.S6B,C). Similar assays using a GST-tagged WASH construct that spans the FAM21 (WHD1) and α-tubulin (WHD2) binding domains (Fig.S6B) confirmed its ability to associate with CCDC28B (Fig.6H). Taken together, these results indicate that CCDC28B couples FAM21/WASH to VPS35 through an interaction involving the C-terminal portion of the multiple repeat-domain of FAM21, where the molecular determinant for its interaction with retromer and EE association also maps[26].

T cells from CVID patients carrying the C211T variant of *ccdc28b* form dysfunctional immune synapses

Having demonstrated that CCDC28B participates in IS assembly and elucidated the underlying mechanism, we addressed the pathogenic potential of the CVID-associated *ccdc28b* C211T SNP. The analysis was carried out on 7 CVID patients carrying one C211T *ccdc28b* allele (P6-P12) and 5 CVID patients homozygous for the wild-type allele (P1-P5) (Table 1). Four healthy donors (HD) were included in the analysis. Proliferation assays of PBMCs in response to plate-bound anti-CD3 mAb showed defective T-cell responses in all patients carrying the R25W variant (P6-P12), who were on this basis classified as T-CVID. Four of the 5 patients homozygous for the wild-type allele (P1-P4) were also T-CVID and were used as disease controls. The remaining patient (P5) was classified as non-T-CVID based on a normal T cell

proliferative response to TCR engagement (Fig.7A). Surface CD3 was comparable among all individuals (Fig.S8A) as were the total levels of CCDC28B (Fig.S8B).

Purified peripheral T cells from all individuals were assessed for their ability to assemble immune synapses with SEA/SEB/SEE-pulsed Raji cells. Confocal immunofluorescence analysis showed that, similar to CCDC28 KD T cells, TCR and tyrosine phosphoprotein accumulation at the T-cell contact with the APC was profoundly impaired in T cells from all patients carrying the C211T *ccdc28b* allele compared to healthy controls (Fig.7B,C). The efficiency of IS formation (% IS) was reduced also in the T-CVID patients carrying the wild-type allele, consistent with the TCR signaling defects associated with T-CVID[7-10]. However, the defect was milder compared to T-CVID expressing CCDC28B^{R25W} (Fig.7B,C). No defect was observed in the CVID patient with normal TCR-dependent T cell proliferation (P5; Fig.S8C). Centrosome polarization was normal in all patients (Fig.7D).

To understand whether the defects in IS assembly were caused by heterozygosity for the C211T *ccdc28b* allele, T cells from all individuals were transfected with a construct encoding GFP-tagged wild-type CCDC28B or the empty GFP construct as control. Overexpression of wild-type CCDC28B fully restored the ability of CCDC28B^{R25W}-expressing T-CVID T cells to form functional immune synapses, as assessed by the synaptic accumulation of CD3 and PTyr (Fig.7E). No significant effect was observed on healthy donor T cells, while a small, yet significant increase in the efficiency of IS formation was observed in T-CVID T cells homozygous for wild-type *ccdc28b* (Fig.7E). Hence heterozygosity for the C211T *ccdc28b* allele strongly impairs the ability of T-CVID T cells to assemble functional immune synapses, supporting its pathogenicity.

To address the underlying mechanism, we asked whether heterozygosity of the C211T *ccdc28b* allele in T-CVID T cells leads to the F-actin phenotypes observed in CCDC28 KD T cells (see figures 4 and S3). A defect in synaptic F-actin accumulation was observed in T cells from these patients (Fig.7F). Of note, similar to CCDC28B-deficient T cells, the proportion of endosomes carrying tCD3 and positive F-actin, WASH or FAM21, as well as the co-localization of tCD3 with these molecules, was profoundly impaired in T cells from the patients carrying the C211T *ccdc28b* allele compared to healthy donor T cells (Fig.7G-I).

Consistent with the impairment in TCR signaling[7-10], synaptic F-actin accumulation was impaired also in T cells from T-CVID patients homozygous for the wild-type allele (Fig.7F). F-actin accumulation at endosomal TCRs was also reduced in these cells, albeit to a lesser extent compared to their CCDC28B^{R25W}-expressing counterparts (Fig.7G). However, these cells showed no defects either in the co-localization of WASH or FAM21 with tCD3, or in the proportion of tCD3^{+} endosomes positive for WASH (Fig.7H,I), with only a partial reduction in the efficiency of FAM21 recruitment to endosomal TCRs (Fig.7I), suggesting that an alternative pathway of local actin polymerization may be affected in T-CVID patients homozygous for the wild-type *ccdc28b* allele.

Together, these data indicate that expression of CCDC28B^{R25W} in T-CVID T cells leads to dysfunctional immune synapses by impairing the ability of wild-type CCDC28B to recruit FAM21/WASH to recycling TCRs, thereby inhibiting local F-actin polymerization.

The CCDC28B residue mutated in CVID is required for coupling FAM21/WASH to the retromer complex

The investigate how CCDC28B^{R25W} uncouples recycling TCRs from FAM21/WASH we transfected Jurkat cells, which carry the wild-type *ccdc28b* allele, with a GFP-tagged construct encoding CCDC28B^{R25W}, reproducing the condition of heterozygosity found in the patients (Fig.8A). CCDC28B^{R25W} expression impaired IS assembly in these cells, as assessed by the defective synaptic accumulation of TCRs and phosphoproteins (Fig.8B,C). Expression of CCDC28B^{R25W} also led to an abnormal F-actin phenotype, as shown by the defect in F-actin accumulation at the IS (Fig.8D). Of note, similar to the CCDC28B^{R25W}-expressing T-CVID T cells, expression of CCDC28B^{R25W} in Jurkat cells phenocopied the effect of CCDC28B KD or KO, impairing the association of both FAM21 and WASH with tCD3^{+} endosomes and the accumulation of F-actin thereon (Fig.8E-G). These results highlight residue R25 as a critical molecular determinant in CCDC28B-dependent FAM21/WASH recruitment to recycling TCRs.

We asked whether the CVID-associated C211T *ccdc28b* allele would impact on the ability of CCDC28B to establish interactions with FAM21/WASH or the retromer complex in T cells. Immunoblot analysis of GFP-specific immunoprecipitates from Jurkat cells transfected with constructs encoding wild-type CCDC28B or CCDC28B^{R25W} revealed that the R25W substitution compromised the interaction of CCDC28B with FAM21 and WASH without affecting its interaction with VPS35

(Fig.8H). These results were confirmed by pull-down assays using GST-tagged CCDC28B^{R25W} (Fig.8I; Fig.S6B). Hence CCDC28B couples FAM21/WASH to the retromer complex through R25.

Similar to other CCDC proteins, CCDC28B has a CC domain that has been implicated in interactions with endosomal membranes for other family members[31]. We hypothesized that the CC domain might be responsible for coupling CCDC28B to the retromer complex at EEs. To address this issue we generated a GST-tagged construct encoding the isolated CC domain of CCDC28B, as well as a construct selectively lacking the CC domain (ΔCC-CCDC28B) (Fig.S6B). VPS35 was pulled down by the GST-tagged CC domain, while the interaction of CCDC28B with VPS35 was lost in the absence of its CC domain (Fig.8I). Consistent with the finding that CCDC28B interacts with FAM21/WASH through R25 in its N-terminal domain, FAM21 and WASH were pulled down by the ΔCC-CCDC28B GST fusion but not by the isolated CC domain (Fig.8I). Hence CCDC28B exploits its CC domain to interact with retromer, and the molecular determinant containing R25 to recruit FAM21-WASH. The interactions are summarized in Figure S6D.

DISCUSSION

Starting from the finding of an increased frequency of the potentially pathogenic C211T SNP in the gene encoding the ciliopathy-related protein CCDC28B in a cohort of 101 CVID patients, and based on the implication of ciliogenesis proteins in IS assembly, here we investigated the role of CCDC28B in this process. We show that CCDC28B participates in IS assembly by promoting actin polymerization at endosomal TCRs, a function involving CCDC28B-mediated recruitment of the actin regulator WASH and its interactor FAM21 to retromer at early endosomes (schematized in Fig.S9). We provide evidence that this function maps to the C211T SNP in *ccdc28b* and that the resulting non-conservative R25W substitution compromises its function.

Polarized recycling from an intracellular endosome-associated pool is a key mechanism exploited by T cells to replenish the IS with TCRs as exhausted receptors are internalized, which allows for sustained signaling during the extended timeframe required for T-cell activation[13,14]. The trafficking machinery responsible for TCR internalization at the plasma membrane, sorting at EEs, and recycling to the cell surface has been delineated in recent years[14]. Here we identify CCDC28B as a new player in the TCR trafficking pathway that acts at EEs, where it couples FAM21 and its binding partner WASH to retromer to promote local actin polymerization (Fig.S6D). This process has been demonstrated to provide the traction force for the abscission of cargo-enriched vesicles that are destined to undergo either recycling to the plasma membrane (e.g. TCR) or retrograde transport to the Golgi apparatus (e.g. the cation-independent mannose 6-phosphate receptor)[26]. FAM21 and WASH also contribute to the transport of these vesicles by tethering them to microtubules through their

respective tubulin-binding domain[26,27]. Interestingly, we found that the ability of CCDC28B to recruit FAM21/WASH to retromer is dependent on R25 within the N-terminal disordered domain of the protein, which is mutated in the C211T *ccdc28b* CVID-associated variant. We mapped this interaction to the C-terminal portion of the multiple repeat domain of FAM21, which is responsible for its association with retromer at EEs[26,29,30]. In turn, binding of CCDC28B to VPS35/retromer requires the C-terminal part of the protein that includes a CC domain, a domain typically involved in protein-protein interactions[31].

It is noteworthy that, while we show that CCDC28B is essential for polarized TCR recycling to the IS, the recycling-related role of CCDC28B might extend to other receptors (e.g. the glucose transporter GLUT1, the chemokine receptor CXCR4) or membrane-associated signaling mediators (e.g. Lck, LAT, Rac1) that are associated with recycling endosomes and participate in IS assembly[32-36]. CCDC28B-deficient T cells display indeed a general defect in endosome polarization downstream of centrosome translocation to the subsynaptic area, concomitant with a defect in the recruitment of the FAM21/WASH complex to EEs and in the resulting local actin polymerization.

ccdc28b was first identified in a screen for disease modifying-genes in Bardet-Biedl syndrome, a pleiotropic genetic disorder associated with defects in the assembly and function of primary cilia[19]. The core complex of BBS proteins, known as the BBSome, controls primary cilium biogenesis by regulating ciliary protein trafficking into this organelle and signaling by the cilium-associated Wnt and Sonic Hedgehog pathways[37]. CCDC28B interacts and colocalizes with all core BBS proteins at the

basal body of ciliated cells[23]. *ccdc28b* knockdown has been shown to result in impaired cilium elongation both in cultured cells and *in vivo* in zebrafish, and in developmental defects that recapitulate BBS phenotypes[24]. These observations, taken together with the epistatic effect of heterozygous *ccdc28b* mutations on disease severity in BBS[19], have led to the hypothesis that CCDC28B may facilitate BBSome function, however the underlying mechanism is as yet unknown. Interestingly, recycling has been suggested as one of the mechanisms for targeting proteins destined for the cilium to the basal body[38]. Our finding that CCDC28B plays a trafficking-related function in the non-ciliated T cell, promoting polarized TCR recycling to the IS, suggests that it may participate in BBSome-dependent protein transport to the cilium. Of note, a recent report has provided evidence for abnormalities in immune cell development in BBS patients[39], suggesting that *ccdc28b* might act as a disease modifier also in the context of these immune-related defects. It will be interesting to assess these patients for the presence of pathogenic *ccdc28b* SNPs.

The genetic aetiology of CVID still poses a formidable challenge. The heterogeneity of clinical presentations and immune cell defects suggests a multigenic origin, which is supported by the growing number of disease genes identified to date, which directly or indirectly affect the maturation of class-switched antibody-producing plasma cells[40]. A significant proportion of CVID patients presents with defects in T-cell activation and helper function[2], which in a subset of patients have been associated with mutations in the T-cell costimulator ICOS[5]. Here we show that T cells from CVID patients heterozygous for the C211T *ccdc28b* allele display defective proliferative responses to TCR stimulation, which can be accounted for by their inability to form functional immune synapses. We have causally linked this defect to an impairment in actin

polymerization at endosomal TCR, which is caused by defective local recruitment of FAM21/WASH to retromer through a molecular determinant that contains R25 and is responsible for the ability of CCDC28B to interact with FAM21. The fact that this interaction is impaired in T cells co-expressing wild-type CCDC28B suggests that CCDC28B^{R25W} functions as a dominant negative mutant. The pathogenic role of this SNP is supported by the fact that forced expression of wild-type CCDC28B in T cells from these patients rescues the IS abnormalities. While this finding highlights *ccdc28b* as a potential new disease gene in T-CVID, it should be pointed out that the C211T SNP is also present in the healthy population, albeit at a lower frequency. This suggests that this *ccdc28b* allele might interact epistatically with other deleterious gene mutations to modify disease presentation or penetrance, similar to BBS[19]. We did not observe any correlation with clinical presentation or the presence of known gene mutations associated with CVID in our patient cohort, however the small number of patients carrying this SNP (9/101) warrants extending the analysis to a larger patient cohort.

It is noteworthy that T cells from T-CVID patients homozygous for wild-type *ccdc28b* also display IS defects, which is consistent with the fact that TCR signaling is impaired in these patients[7-10]. However, while F-actin accumulation at TCR complexes undergoing recycling is defective in T cells from these patients, the FAM21/WASH-dependent pathway that regulates F-actin polymerization on endosomal TCRs appears to be largely unaffected, suggesting the existence of an alternative pathway that regulates this process and is impaired in T-CVID T cells homozygous for wild-type *ccdc28b*. Of note, we observed that the IS assembly defects in these T-CVID T cells were attenuated to a limited extent when wild-type CCDC28B was overexpressed. The

C430T *ccdc28b* variant associated to BBS has been shown to enhance the usage of a cryptic splice acceptor site that introduces a premature termination codon[19], indicating a gene dosage effect. We hypothesize that increasing the total complement of wild-type CCDC28B in these T-CVID T cells could partially compensate for the defect in the putative alternative pathway of endosomal F-actin polymerization. Interestingly, mutations in the gene encoding the WASH-related protein WASP have been recently identified in whole-exome sequencing of a large cohort of CVID patients[4], suggesting that multiple gene defects might converge on the process of F-actin polymerization in CVID.

Ciliogenesis proteins have emerged in recent years as important regulators of IS assembly and signaling in T cells. In particular, proteins implicated in the trafficking of building blocks or signaling regulators to the cilium have been demonstrated to regulate the synaptic transport of the TCR as well as membrane-associated signaling components, such as the kinase Lck and the adaptor LAT[21]. The identification of CCDC28B as part of the TCR trafficking machinery provides further evidence of the conservation in the pathways that control IS and primary cilium assembly. Taken together with our finding of an increased frequency of a pathogenic mutation in a ciliary protein in CVID, these data highlight ciliogenesis proteins as promising disease candidates for primary immunodeficiencies or other immune-related disorders associated with dysfunctional immune synapses.

METHODS

Patients and cells

Patients were classified as CVID according to using established criteria[41]. Hematologic and immunophenotypical characterization of patients is shown in Table 1. NGS analysis on these patients ruled out the presence of genes know to be associated with defective B cell function (unpublished results). Peripheral blood mononuclear cells (PBMCs) were isolated from whole blood of healthy donors and CVID patients by density centrifugation on Lympholyte-H Cell Separation Media (Euroclone, Milan, Italy). Experiments were performed after approval by the institutional review board of the Universities of Florence and Brescia for these studies. Peripheral blood was obtained after informed consent according to the Declaration of Helsinki, and sample size was kept small according to the guidelines of the ethics committee. No overt infectious disease was present at the time of blood sampling.

Cells lines included Jurkat T cells, Raji B cells and the BJ-5ta human hTERT-immortalized fibroblast line. Primary T-cells purified from peripheral blood of healthy donors using the Rosette Sep kit followed by density centrifugation on Lympholyte. The latter were expanded by stimulation with 0.1 μg/ml Staphylococcal enterotoxin E (SEE), B (SEB) and A (SEA) (Toxin Technology, Sarasota, FL, USA) and 130 U/ml human IL-2 (Miltenyi Biotec) for 7–10 days (Fig.S4A) in order to increase the number of antigen-specific T-cells.

Antibodies, reagents, plasmid and GST fusions

IgG from OKT3 (anti-human CD3ε, IgG2) hybridoma supernatants was purified using Mabtrap (Amersham Biosciences, Inc., Piscataway, NJ, USA) and titrated by flow

cytometry. All primary commercial antibodies used in this work are listed in Table S1, together with information about the dilutions used for immunoblotting, immunofluorescence and immunoprecipitation. Secondary peroxidase-labeled antibodies were from Amersham Biosciences, Alexa Fluor 488- and 555-labeled secondary Abs from Molecular Probes (Invitrogen, Eugene, OR, USA). Cell Tracker Blue was from Molecular Probes (Invitrogen) and poly-L-lysine from Sigma-Aldrich. 16% Formaldehyde was from Thermo Scientific.

GFP-tagged wild-type CCDC28B (wt) was obtained by cloning CCDC28B wt cDNA in pEGFP-N1 digested with XhoI and BamHI restriction enzymes (Thermo Fisher Scientific, Waltham, MA USA). GFP-tagged CCDC28B^{R25W} (mut) was obtained using the QuikChange II site-directed mutagenesis kit (Agilent, Santa Clara, USA) and the mutated sequence was verified by DNA sequencing (Bio-Fab, Rome, Italy). Primers used for cloning are listed in Table S2.

The GST-tagged proteins used in this study are schematized in figure S5B. The constructs encoding the GST-tagged N- and C-terminal portions of the FAM21 multiple repeat domain of FAM21 (FAMn and FAMc, respectively) and GST-tagged WASH lacking the VCA domain were previously described[26,29]. The cDNAs encoding CCDC28B wt, CCDC28B mut, CCDC28B depleted of the coiled-coil domain (ΔCC) and the CCDC28B coiled-coil domain (CC) were inserted into the bacterial expression plasmid pGEX-6P-2, using EcoRI and XhoI restriction enzymes (Thermo Fisher Scientific, Waltham, MA USA). The recombinant fusion proteins, as well as control GST, were affinity purified on GSH-Sepharose (GE Healthcare) from bacterial cultures incubated for 4 h at 37°C with 0.25 mM isopropyl-β-D-thiogalactopyranoside and lysed by sonication in PBS-1% Triton X-100.

DNA extraction, NGS analysis and PCR sequencing

DNA was extracted from peripheral blood from CVID patients using QIAamp DNA Mini Kit or QIAmp Blood DNA Mini Kit (Qiagen GmbH, Hilden, Germany). The extraction was performed according to the manufacturer's instructions for genomic DNA purification from blood. Quality control of DNA samples from 7 T-CVID patients and high-coverage NGS analysis of the exons of approximately 100 genes encoding proteins implicated in ciliogenesis, vesicular trafficking and TCR signaling were performed by Oxford Gene Technology-The Molecular Genetics Company™ (Begbroke, Oxfordshire, UK) (unpublished results). Variants were annotated with gene and gene function data from Ensembl[42]. Allele frequencies in the matched ethnic group were from 1000 Genomes Project Phase 3[43] (Central European) and the Genome Aggregation database (gnomAD; Broad Institute)[44]. Variants of 5 ciliopathy-related gene variants predicted as likely to cause significant functional problems were analyzed by classical Polymerase Chain Reaction (PCR) and Sanger sequencing in a cohort of 101 CVID patients. PCR reactions were performed using Go Taq Long Pcr Master Mix 2X (Promega) and primer pairs reported in Table S2. Sequence reactions were performed by Bio-Fab research Srl (Roma, Italy).

Transfections, RNA interference and CRISPR-Cas9 mutagenesis

Jurkat cells or primary T cells were transiently transfected by electroporation with human CCDC28B-specific esiRNAs (EHU082341) (KD) and unrelated control esiRNA (EHURLUC) (ctr) (150ng/10^6 cells) (Sigma-Aldrich, Milan, Italy) and assays were carried out after 48 h. Rescue experiments were performed by transfecting CCDC28B KD Jurkat cells with GFP-tagged wt CCDC28B (1µg/10^6 cells) by electroporation and assays were carried out after 24 h. Transient transfection of Jurkat T cells with GFP-

tagged wt or mut CCDC28B (1µg/10^6 cells) were performed by electroporation and assays were carried out after 24 h. All the sample were resuspended in OPTI-MEM 1X solution (Gibco) before undergo electroporation using Gene Pulser II (Bio-Rad). To generate CCDC28B KO clones, a guide RNA (gRNA, Table S2) targeting Cas9 nuclease activity to *ccdc28b* was designed using the web-based tool CRISPOR[45] and cloned into the pSpCas9(BB)-2A-GFP (PX458) plasmid (a gift from F. Zhang; Addgene, 48138) as described elsewhere[46]. Jurkat cells were transfected with either empty vector or the gRNA-encoding construct using the Nucleofector Solution 2M (5 mM KCl, 15 mM $MgCl_2$, 15 mM HEPES, 150 mM Na_2HPO_4/NaH_2PO_4 pH 7.2, 50 mM Manitol) (Chicaybam et al 2013) and the Amaxa Nucleofector II system (Lonza), Program X-005. GFP-expressing cells were sorted, subcloned, and screened for gene knockout by immunoblotting.

IS formation and TCR recycling assays

Conjugates between Jurkat or blast T cells (freshly purified or blasts, see figure 6A) and superantigen (SAg)-pulsed Raji B cells were carried out as previously described[15]. In conjugates with Jurkat cells, Raji cells (used as APC) were pulsed for 2 h with 10 µg/ml SEE and labeled with 10 µM Cell Tracker Blue for the last 20 min, while for IS experiments with freshly purified or SAg-expanded T cells Raji were pulsed with a mix of SEE, SEA and SEB (10 µg/ml each). Analyzes were carried out 15 min after conjugate formation, with the exception of the analyses shown in figure 2A, which included a shorter time (5 min). Conjugates between T cells and unpulsed B cells, where no IS forms at the interface of the cell pairs, were used as negative controls. Samples were allowed to adhere for 15 min on polylysine-coated wells of diagnostic microscope slides (Erie Scientific Company), fixed by immersion in methanol for 10

min at −20°C, or analyzed under non-permeabilizing conditions after fixation in 4% paraformaldehyde for 20 min at RT. Following fixation, samples were washed in PBS and incubated with primary antibodies (Table S1) overnight at 4°C or 1 h at room temperature. After washing in PBS, samples were incubated for 1 h at room temperature with Alexa-Fluor-488- and -555-labeled secondary antibodies.

For the TCR receptor recycling assays, cells were incubated with saturating concentrations of anti-human CD3ε mAb (clone OKT3) at 37°C for 2 h, washed to remove excess mAb, acid-stripped and used in IS experiments as described above.

Confocal and TIRF immunofluorescence, co-localization analyses

Confocal microscopy was carried out on a Zeiss LSM700 using a 63X objective. Images were acquired with pinholes opened to obtain 0.8-µm-thick sections. Detectors were set to detect an optimal signal below the saturation limits. Images were processed with Zen 2009 image software (Carl Zeiss, Jena, Germany). The quantitative co-localization analysis of CCDC28B with γ-tub, Rab5, Rab11 and GM130 was performed on median optical sections using ImageJ and JACoP plug-in to determine Mander's coefficient M_1[47], which represents the percentage of CCDC28B pixels (red channel) that overlaps γ-tubulin, Rab5, Rab11 or GM130 pixels (green channel) (0=no co-localization; 1=100% co-localization).

Scoring of conjugates for polarized TCR recycling to the IS in permeabilized or non-permeabilized cells as well as for PTyr, CD3ζ and γ-tub clustering at the IS in permeabilized cells was based on the concentration of the respective staining solely at the T-cell–APC contact. Centrosome polarization to the IS, assessed as the reduction of the distance of the centrosome from the APC contact site in T cells exposed to SAg-loaded versus unloaded APC[48], was measured using ImageJ. The

recruitment index was calculated for each marker as the relative fluorescence at the T-cell:APC contact site compared to the remaining T-cell area. For co-localization in conjugates obtained following TCR recycling assays, analyses were performed on single tCD3 dots using ImageJ and JACoP plug-in to determine Manders' coefficient M_1. The same type of analysis was carried out on WASH/F-actin and WASH/Rab5 conjugates, where single $WASH^+$ dots were analyzed, and FAM21/Rab5 conjugates, where $FAM21^+$ dots were analyzed. The distance of $F\text{-}actin^+$ or $WASH^+$ dots from IS was measured using ImageJ.

In TIRF immunofluorescence experiments, F-actin ring formation was evaluated in primary T cells, allowed to adhere for 15 min on cover glass, thickness 0.16 mm (Vwr International Srl, Milan, Italy) coated with purified anti-human CD3ε mAb, clone UCHT1 (Biolegend), fixed in PBS-4% paraformaldehyde methanol free for 15 min at room temperature, permeabilized with PBS-0.25% Triton X-100 for 15 min and stained with Alexa Fluor 488 phalloidin (Invitrogen) in PBS-1% BSA for 30 min. TIRF images were acquired on an inverted Leica DMi8 microscope (Leica Microsystem), with 63X objectives using a PCO Edge sCMOS camera (Leica Microsystems). Spreading areas were measured using ImageJ.

Flow cytometry

Protein tyrosine phosphorylation was analyzed by flow cytometry in conjugates of control or CCDC28B KD Jurkat cells and SEE-pulsed Raji cells (APC), at different time points. Conjugates were labelled with PE-labelled anti-human CD3 mAb (CD3ε, clone OKT3) (Biolegend) and anti-PTyr antibodies (Merk Millipore) and $CD3^+$ cells were analyzed. F-actin was quantified by flow cytometry in primary T cells stimulated with purified anti-human CD3ε mAb, clone UCHT1 (Biolegend) for 15 min at 37°C, fixed

and permeabilized using Cytofix/Cytoperm Plus kit (Becton Dickinson, San Jose, CA) and stained with Alexa Fluor 488 phalloidin (Invitrogen). F-actin content was calculated as fold increase of stimulated versus unstimulated samples. CD3 surface expression on Jurkat cells KD or KO for CCDC28B expression, primary T cells KD for CCDC28B and their respective controls, and PBMCs from CVID patients and healthy donors, was measured by flow cytometry using PE-labelled anti-human CD3 mAb (CD3ε, clone OKT3) (Biolegend). Flow cytometry was carried out using a Guava Easy Cyte cytometer (Millipore).

For proliferation assays, PBMCs from CVID patients and healthy donors were stimulated with plate-bound anti-CD3ε mAb (OKT3) and processed 16-48 h after activation. [^{3}H]-thymidine (1 mCi) was added to each well for the last 18 h of culture. After harvesting the cells with an automatic harvester, proliferation was determined by measuring the [^{3}H]thymidine incorporation in a liquid scintillation counter.

Immunoprecipitations, immunoblots and *in vitro* binding assays

For immunoprecipitation experiments, cells (5x10^7/sample) were pelleted, washed twice in ice-cold PBS and lysed in 500 µl lysis buffer (0.5% Triton X-100 in 20 mM Tris-HCl, pH 8.0, 150 mM NaCl) in the presence of protease inhibitors (Calbiochem, 539,134) and the phosphatase inhibitor sodium vanadate (Sigma-Aldrich, S6508). Quantification was carried out using the BCA Assay kit (EuroClone, EMP014500). Postnuclear supernatants were immunoprecipitated using the appropriate antibodies (see Table S1) or mouse IgG isotype control (Invitrogen) and protein A Sepharose (GE Healthcare). PAS-antibody complexes were pelleted, washed 4X with 1 ml lysis buffer, then resuspended in 15 µl Laemmli buffer (LifeTechnologies, B0007), boiled for 5 min and subjected to SDS-PAGE. All gels included a sample of the lysates used

for the immunoprecipitations (50 µg/sample). *In vitro* binding assays were carried using the GST-tagged proteins on GSH-Sepharose-precleared postnuclear supernatants from $5x10^7$cells/sample, lysed in 1% Triton X-100 in the presence of protease inhibitors. Immunoblotting was carried out using peroxidase-labeled secondary Ig and a chemiluminescence detection kit (Pierce Rockford). Stripping was carried out by using ReBlot Plus Mild Antibody Stripping Solution, 10x (Chemicon). Blots were scanned using a laser densitometer (Duoscan T2500; Agfa, Milan, Italy) and quantified using ImageJ.

Statistical analysis

Mean values, standard deviation values and Student's t test (unpaired) were calculated using the Microsoft Excel application. For patients data where multiple groups were compared One-way ANOVA was used. Mann-Whitney rank-sum tests were performed to determine the significance of the differences between two groups. Statistical analyses were performed using GraphPad Software (La Jolla, CA). A P-value of <0.05 was considered as statistically significant.

Acknowledgements

We wish to thank Claire Hivroz for critical reading of the manuscript and Vincenzo Sorrentino for useful advice. This work was carried out with the support of Fondazione Telethon, Italy (Grant GGP16003) to CTB.

Author contributions

NC, AO, FF, CC and CTB designed research and analyzed and interpreted data; NC, AO, FF, CC and JB carried out the experiments; VL, AT, SD, MB, LG, DDB, MMD and AP contributed vital reagents; NC and CTB drafted the manuscript.

Competing interests

The authors declare no competing financial interests.

Data availability

The datasets generated during and/or analysed during the current study are available from the corresponding author on reasonable request.

REFERENCES

1. Resnick, E.S. & Cunningham-Rundles, C. The many faces of the clinical picture of common variable immune deficiency. *Curr Opin Allergy Clin Immunol* **12**, 595-601 (2012).
2. Yazdani, R., Hakemi, M.G., Sherkat, R., Homayouni, V. & Farahani, R. Genetic defects and the role of helper T-cells in the pathogenesis of common variable immunodeficiency. *Adv Biomed Res* **3**, 2 (2014).
3. Orange, J.S. *et al.* Genome-wide association identifies diverse causes of common variable immunodeficiency. *J Allergy Clin Immunol* **127**, 1360-1367 e1366 (2011).
4. Abolhassani, H., Hammarstrom, L. & Cunningham-Rundles, C. Current genetic landscape in common variable immune deficiency. *Blood* **135**, 656-667 (2020).
5. Grimbacher, B. *et al.* Homozygous loss of ICOS is associated with adult-onset common variable immunodeficiency. *Nat Immunol* **4**, 261-268 (2003).
6. Lougaris, V. *et al.* A de novo monoallelic CTLA-4 deletion causing pediatric onset CVID with recurrent autoimmune cytopenias and severe enteropathy. *Clin Immunol* **197**, 186-188 (2018).
7. Fischer, M.B. *et al.* Activation via the antigen receptor is impaired in T cells, but not in B cells from patients with common variable immunodeficiency. *Eur J Immunol* **26**, 231-237 (1996).
8. Majolini, M.B. *et al.* Uncoupling of T-cell antigen receptor and downstream protein tyrosine kinases in common variable immunodeficiency. *Clin Immunol Immunopathol* **84**, 98-102 (1997).

9. Boncristiano, M. *et al.* Defective recruitment and activation of ZAP-70 in common variable immunodeficiency patients with T cell defects. *Eur J Immunol* **30**, 2632-2638 (2000).
10. Paccani, S.R. *et al.* Defective Vav expression and impaired F-actin reorganization in a subset of patients with common variable immunodeficiency characterized by T-cell defects. *Blood* **106**, 626-634 (2005).
11. Capitani, N. *et al.* Vav1 haploinsufficiency in a common variable immunodeficiency patient with defective T-cell function. *Int J Immunopathol Pharmacol* **25**, 811-817 (2012).
12. Dustin, M.L. & Choudhuri, K. Signaling and Polarized Communication Across the T Cell Immunological Synapse. *Annu Rev Cell Dev Biol* **32**, 303-325 (2016).
13. Soares, H., Lasserre, R. & Alcover, A. Orchestrating cytoskeleton and intracellular vesicle traffic to build functional immunological synapses. *Immunol Rev* **256**, 118-132 (2013).
14. Onnis, A. & Baldari, C.T. Orchestration of Immunological Synapse Assembly by Vesicular Trafficking. *Front Cell Dev Biol* **7**, 110 (2019).
15. Finetti, F. *et al.* Intraflagellar transport is required for polarized recycling of the TCR/CD3 complex to the immune synapse. *Nat Cell Biol* **11**, 1332-1339 (2009).
16. Finetti, F. *et al.* The small GTPase Rab8 interacts with VAMP-3 to regulate the delivery of recycling T-cell receptors to the immune synapse. *J Cell Sci* **128**, 2541-2552 (2015).
17. Onnis, A. *et al.* The small GTPase Rab29 is a common regulator of immune synapse assembly and ciliogenesis. *Cell Death Differ* **22**, 1687-1699 (2015).
18. Vivar, O.I. *et al.* IFT20 controls LAT recruitment to the immune synapse and T-cell activation in vivo. *Proc Natl Acad Sci U S A* **113**, 386-391 (2016).

19. Badano, J.L. *et al.* Dissection of epistasis in oligogenic Bardet-Biedl syndrome. *Nature* **439**, 326-330 (2006).

20. Cardenas-Rodriguez, M. *et al.* Characterization of CCDC28B reveals its role in ciliogenesis and provides insight to understand its modifier effect on Bardet-Biedl syndrome. *Hum Genet* **132**, 91-105 (2013).

21. Cassioli, C. & Baldari, C.T. A Ciliary View of the Immunological Synapse. *Cells* **8** (2019).

22. Das, V. *et al.* Activation-induced polarized recycling targets T cell antigen receptors to the immunological synapse; involvement of SNARE complexes. *Immunity* **20**, 577-588 (2004).

23. Granger, E., McNee, G., Allan, V. & Woodman, P. The role of the cytoskeleton and molecular motors in endosomal dynamics. *Semin Cell Dev Biol* **31**, 20-29 (2014).

24. Martin-Cofreces, N.B. & Sanchez-Madrid, F. Sailing to and Docking at the Immune Synapse: Role of Tubulin Dynamics and Molecular Motors. *Front Immunol* **9**, 1174 (2018).

25. Seaman, M.N., Gautreau, A. & Billadeau, D.D. Retromer-mediated endosomal protein sorting: all WASHed up! *Trends Cell Biol* **23**, 522-528 (2013).

26. Gomez, T.S. & Billadeau, D.D. A FAM21-containing WASH complex regulates retromer-dependent sorting. *Dev Cell* **17**, 699-711 (2009).

27. Derivery, E. *et al.* The Arp2/3 activator WASH controls the fission of endosomes through a large multiprotein complex. *Dev Cell* **17**, 712-723 (2009).

28. Wang, J. et al. Endosomal receptor trafficking: Retromer and beyond. *Traffic* **19**, 578-590 (2018).

29. Jia, D., Gomez, T.S., Billadeau, D.D. & Rosen, M.K. Multiple repeat elements within the FAM21 tail link the WASH actin regulatory complex to the retromer. *Mol Biol Cell* **23**, 2352-2361 (2012).

30. Harbour, M.E., Breusegem, S.Y. & Seaman, M.N. Recruitment of the endosomal WASH complex is mediated by the extended 'tail' of Fam21 binding to the retromer protein Vps35. *Biochem J* **442**, 209-220 (2012).

31. Truebestein, L. & Leonard, T.A. Coiled-coils: The long and short of it. *Bioessays* **38**, 903-916 (2016).

32. Ehrlich, L.I., Ebert, P.J., Krummel, M.F., Weiss, A. & Davis, M.M. Dynamics of p56lck translocation to the T cell immunological synapse following agonist and antagonist stimulation. *Immunity* **17**, 809-822 (2002).

33. Bonello, G. *et al.* Dynamic recruitment of the adaptor protein LAT: LAT exists in two distinct intracellular pools and controls its own recruitment. *J Cell Sci* **117**, 1009-1016 (2004).

34. Piotrowski, J.T., Gomez, T.S., Schoon, R.A., Mangalam, A.K. & Billadeau, D.D. WASH knockout T cells demonstrate defective receptor trafficking, proliferation, and effector function. *Mol Cell Biol* **33**, 958-973 (2013).

35. Finetti, F. *et al.* Specific recycling receptors are targeted to the immune synapse by the intraflagellar transport system. *J Cell Sci* **127**, 1924-1937 (2014).

36. Bouchet, J. *et al.* Rac1-Rab11-FIP3 regulatory hub coordinates vesicle traffic with actin remodeling and T-cell activation. *EMBO J* **35**, 1160-1174 (2016).

37. Nachury, M.V. The molecular machines that traffic signaling receptors into and out of cilia. *Curr Opin Cell Biol* **51**, 124-131 (2018).

38. Carter, S.P. & Blacque, O.E. Membrane retrieval, recycling and release pathways that organise and sculpt the ciliary membrane. *Curr Opin Cell Biol* **59**, 133-139 (2019).

39. Tsylakuri, O. *et al*. Altered hematopoietic system and self-tolerance in Bardet-Biedl Syndrome. BioRxiv 962886 [preprint]. February 25, 2020. doi: https://doi.org/10.1101/2020.02.24.962886.

40. Romberg, N. & Lawrence, M.G. Birds of a feather: Common variable immune deficiencies. *Ann Allergy Asthma Immunol* **123**, 461-467 (2019).

41. Tangye, S.G. et al. Human Inborn Errors of Immunity: 2019 Update on the Classification from the International Union of Immunological Societies Expert Committee. *J Clin Immunol* **40**, 24-64 (2020)

42. Yates, A.D. *et al.* Ensembl 2020. *Nucleic Acids Res* **48**, D682-D688 (2020).

43. Genomes Project, C. *et al.* A global reference for human genetic variation. *Nature* **526**, 68-74 (2015).

44. Karczewski, K.J. *et al.* The mutational constraint spectrum quantified from variation in 141,456 humans. *Nature* **581**, 434-443 (2020).

45. Haeussler, M. *et al.* Evaluation of off-target and on-target scoring algorithms and integration into the guide RNA selection tool CRISPOR. *Genome Biol* **17**, 148 (2016).

46. Ran, F.A. *et al.* Genome engineering using the CRISPR-Cas9 system. *Nat Protoc* **8**, 2281-2308 (2013).

47. Manders, E.M., Stap, J., Brakenhoff, G.J., van Driel, R. & Aten, J.A. Dynamics of three-dimensional replication patterns during the S-phase, analysed by double labelling of DNA and confocal microscopy. *J Cell Sci* **103 (Pt 3)**, 857-862 (1992).

48. Esquerre, M. *et al.* Human regulatory T cells inhibit polarization of T helper cells toward antigen-presenting cells via a TGF-beta-dependent mechanism. *Proc Natl Acad Sci U S A* **105**, 2550-2555 (2008).

Table 1. Immunological and clinical data from CVID patients P1-P12* (Figures 7 & S8)

	P1	P2	P3	P4	P5	P6	P7	P8	P9	P10	P11	P12
Sex	F	M	M	M	M	F	F	F	M	F	F	M
Age (onset/current)	23/53	25/57	1/34	1/40	2/38	29/65	9/20	24/48	2/25	26/47	11/34	3/15
Age (diagnosis and evaluation)	36	34	15	8	9	37	11	38	16	38	25	8
WBCs (cell/μl)	6360	7280	10610	7730	5700	5120	7150	7170	5790	6270	7800	6420
Neutrophils (cells/μl)	3310	4490	2472	4638	3819	2740	3780	4800	2450	4100	4524	3120
Lymphocytes (cells/μl)	3175	2840	4498	2164	1482	1700	2245	2354	1800	1300	3198	2780
Platelets (cells/μl)	190000	252000	590000	160000	347000	210000	147000	238000	180000	253000	268000	191000
IgG (mg/dl)	270	301	235	239	432	224	462	280	330	180	412	384
IgA (mg/dl)	8	6	<5	18	184	4	34	8	10	<5	4	6
IgM (mg/dl)	9	11	60	46	24	5	6	<5	26	<6	3	12
Anti-tetanus toxoid antibodies (UI/ml)	neg	neg	neg	neg	neg	neg	neg	neg	neg	neg	neg	neg
Anti-Hepatitis antibodies (UI/ml)	neg	neg	neg	neg	neg	neg	neg	neg	neg	neg	neg	neg
T cells ($CD3^+$) (%)	79	83	52	71	91	68	84	74	72	90	64	73
$CD3^+CD4^+$	51	30	22	28	19	49	51	30	45	42	37	39
$CD3^+CD8^+$	28	39	26	32	52	17	28	39	15	28	20	28
B cells ($CD19^+$) (%)	7	6	42	10	1	9	3	5	14	6	23	13

NK cells ($CD3^-$ $CD16^+CD56^+$) (%)	8	11	3	15	7	9	13	16	12	12	6	12
Recurrent respiratory infections	+	+	+	+	+	+	+	+	+	+	+	+
Bronchiectasis	-	+	*	-	-	+	-	+	-	+	-	+
Lymphoadenopathy	+	-	+	+	+	+	+	-	-	-	-	-
Splenomegaly	-	-	+**	+	+	-	+	-	-	-	+	-
Autoimmune cytopenias	-	+	+	-	-	-	+	-	-	-	-	-
Autoimmune enteropathy	-	-	-	-	-	-	-	-	-	-	-	-
Other	-	-	Celiac disease, MALT lymphoma; giardia lamblia gi infections	-	Folliculitis; eczema	*H.pylori* gastric adenocarcinoma	Chronic CMV infection	-	-	-	Thalassemia major	-

* negative for mutations in ~ 60 genes associated with B cell defects as assessed by NGS (not shown)
** splenectomized at the age of 8

FIGURE LEGENDS

Figure 1. CCDC28B is expressed in T cells and is recruited to the IS. A. Sanger sequencing chromatograms of the PCR amplification products of *ccdc28b* (NG_012178.1, nucleotide positions 6289-6510, corresponding to cDNA nucleotide positions 116-302, covering the entire exon 2) on genomic DNA from representative CVID patients carrying either the wild-type ccdc28b allele (left) or heterozygous for the C211T allele (right). A scheme of the domain organization of CCDC28B is shown below. **B.** Representative immunoblot of CCDC28B in lysates of hTERT-immortalized fibroblasts, Jurkat T cells and primary T cells. **C,D**. Immunofluorescence analysis and co-localization of CCDC28B and in Jurkat cells costained with antibodies to γ-tubulin (centrosome), Rab5 (early endosome), Rab11 (recycling endosome) or GM130 (Golgi apparatus). Representative images (medial optical sections) are shown in C. The quantification (mean±SD) using Mander's coefficient of the weighted co-localization of CCDC28B with each marker is shown in D. 30 cells were analyzed for each marker (n=3). **E,F**. Immunofluorescence analysis of CCCDC28B and γ-tubulin in conjugates of Jurkat cells and SEE-pulsed Raji cells (APC) (E), or primary T cells and Raji cells pulsed with a mix of SEA, SEB and SEE (SAg) (F). Conjugates formed in the absence of SEE/SAg were used as negative controls. Representative images (medial optical sections) are shown (n=3). Size bar, 5 μm.

Figure 2. CCDC28B is required for immune synapse assembly. A. Immunofluorescence analysis of CD3ζ (top), tyrosine phosphoproteins (PTyr) (middle) or γ-tubulin (bottom) in 15-min conjugates of control or CCDC28B KD Jurkat cells and SEE-pulsed Raji cells (APC). The histograms show the quantification (%) of

conjugates with CD3ζ, PTyr or γ-tubulin staining at the T cell:APC contact site 5 min and 15 min after conjugate formation. At least 100 conjugates were analyzed for each marker (n≥3). **B**. Left, Histograms showing the relative fluorescence of CD3ζ (top; includes membrane and endosomal CD3ζ) or PTyr (bottom) at the T-cell:APC contact site compared to the remaining T-cell area (recruitment index). Right, histogram showing the mean distance of $CD3\zeta^+$ endosomes (eCD3, top) or of the centrosome (γ-tub, bottom) from the T-cell:APC contact site (μm). Measurements were taken on 50 conjugates (n≥3). **C.** Immunofluorescence analysis of CD3ζ (top), tyrosine phosphoproteins (PTyr) (middle) or γ-tubulin (bottom) in conjugates of control or CCDC28B KD primary T cells cells and Raji cells (APC) pulsed with a mix of SEA, SEB and SEE. The histograms show the quantification (%) of conjugates with CD3ζ, PTyr or γ-tubulin staining at the IS 15 min after conjugate formation. At least 100 conjugates were analyzed for each marker (n≥3). **D**. Histograms showing the quantification (%) of 15-min conjugates with CD3ζ, PTyr or γ-tubulin staining at the IS in conjugates of control or CCDC28B KD Jurkat cells, transfected with either empty vector (ctr, KD) or the same vector encoding wild-type CCDC28B (KD+CCDC28B), and SEE-pulsed Raji cells. At least 50 conjugates were analyzed for each marker (n≥3). Size bar, 5 μm. Error bars, SD. ***, $p<0.001$; **, $p<0.01$; *, $p<0.05$ (Student's t-test).

Figure 3. CCDC28B is required for polarized TCR recycling to the IS. A,B. Immunofluorescence analysis of recycling TCRs (tCD3) in control or CCDC28B KD Jurkat cells conjugated for 15 min with SEE-pulsed Raji cells (APC) (A) or primary T cells conjugated with SEA/SEB/SEE-pulsed Raji cells (B). Before conjugation, cells were added with anti-CD3ε mAb (OKT3) and incubated at 37°C for 2 h to allow for

internalization of CD3-Ab complexes. Following acid-stripping to remove residual anti-CD3 mAb bound at the cell surface. Conjugates were stained with secondary fluorescently-labelled antibodies, after fixing either under non-permeabilizing conditions (top) or after cell permeabilization (bottom). The histograms show the quantification (%) of conjugates with tCD3 at the IS (left). The histograms on the right show either the relative fluorescence of tCD3 at the T-cell:APC contact site compared to the remaining T-cell area (recruitment index) for non-permeabilized conjugates, or the mean distance of $tCD3^+$ endosomes from the T-cell:APC contact site (μm) for permeabilized conjugates. At least 20 conjugates were analyzed in each experiment (n≥3). Size bar, 5 μm. Error bars, SD. ***, p<0.001; **, p<0.01; *, p<0.05 (Student's t-test).

Figure 4. CCDC28B is required for TCR-dependent F-actin polymerization. A. Flow cytometric analysis of F-actin polymerization in response to TCR engagement in phalloidin-stained control or CCDC28B KD Jurkat cells. Cells were stimulated with soluble anti-CD3ε mAb (UCHT-1) for 15 min. The data are expressed as fold increase of F-actin in stimulated vs non-stimulated cells (n=3). **B.** TIRF microscopy-based analysis of F-actin in phalloidin-stained control or CCDC28B KD Jurkat cells activated by plating on anti-CD3ε mAb (UCHT-1)-coated coverslips for 15 min. The histogram shows the cell area (μm^2) as a measure of cell spreading (n cells=20, n=3). **C,D**. Immunofluorescence analysis of F-actin in 15 min-conjugates of control or CCDC28B KD Jurkat cells and SEE-pulsed Raji cells (APC) (C), or control or CCDC28B KD primary T cells and SEA/SEB/SEE-pulsed Raji cells (D) stained with fluorochrome-tagged phalloidin. The histograms show the quantification (%) of conjugates with F-actin staining at the IS (at least 100 conjugates were analyzed, n≥3) (left) or the relative

fluorescence of F-actin at the T-cell:APC contact site compared to the remaining T-cell area (recruitment index) (n=25 conjugates). **E,F**. Immunofluorescence analysis of recycling TCRs (tCD3) and F-actin in control or CCDC28B KD Jurkat cells conjugated for 15 min with SEE-pulsed Raji cells (APC) (E) or primary T cells conjugated with SEA/SEB/SEE- pulsed Raji cells (F). Before conjugation, cells were added with anti-CD3ε mAb (OKT3) and incubated at 37°C for 2 h to allow for internalization of CD3-Ab complexes. Following acid-stripping to remove residual anti-CD3 mAb bound at the cell surface. Conjugates were permealized/fixed and stained with secondary fluorescently-labelled antibodies and fluorochrome-labelled phalloidin. The histograms show the mean distance of F-actin$^+$ dots from the T-cell:APC contact site (top, μm); the co-localization of tCD3 with F-actin on individual dots (bottom left, Mander's coefficient); and the quantification of tCD3$^+$ dots positive for F-actin (bottom right). Measurements were taken on 50 conjugates from at least 3 independent experiments and a mean of 10 dots per cell were analyzed. Size bar, 5 μm. Error bars, SD. ***, $p<0.001$; **, $p<0.01$; *, $p<0.05$ (Student's t-test).

Figure 5. CCDC28B is required for recruitment of the actin regulator WASH and its adaptor FAM21 to recycling TCRs. A. Immunofluorescence analysis of WASH in 15 min-conjugates of control or CCDC28B KD Jurkat cells and SEE-pulsed Raji cells (APC) co-stained for F-actin. The histograms show the mean distance of WASH$^+$ dots from the T-cell:APC contact site (top) and the quantification of WASH$^+$ dots positive for actin (%, bottom). **B,C**. Immunofluorescence analysis of recycling TCRs (tCD3; see legend to figure 4E for experimental setting) in control or CCDC28B KD Jurkat cells conjugated for 15 min with SEE-pulsed Raji cells (APC) and co-stained for WASH (B) or FAM21 (C). For each panel the histograms show the quantification of tCD3$^+$ dots

positive for WASH or FAM21 (top, %); and the co-localization of tCD3 with WASH or FAM21 on individual dots (bottom, Mander's coefficient). Measurements were taken on 50 conjugates from at least 3 independent experiments and a mean of 10 dots per cell were analyzed. Size bar, 5 µm. Error bars, SD. ***, $p<0.001$; **, $p<0.01$; *, $p<0.05$ (Student's t-test).

Figure 6. CCDC28B associates with recycling TCRs and forms a complex with WASH, FAM21 and VPS35. A-C. Immunofluorescence analysis of WASH (A) and FAM21 (B) in 15 min-conjugates of control or CCDC28B KD Jurkat cells and SEE-pulsed Raji cells (APC) co-stained for Rab5. The histograms show the co-localization of WASH or FAM21 with Rab5 on individual dots (Mander's coefficient). Measurements were taken on 50 conjugates from at least 3 independent experiments and a mean of 10 dots per cell were analyzed. **C**. Immunoblot analysis of tCD3-specific immunoprecipitates from post-nuclear supernatants of control or CCDC28B KD Jurkat cells. Cells were added with anti-CD3ε mAb (OKT3) and incubated at 37°C for 2 h to allow for internalization of CD3-Ab complexes. Following acid-stripping to remove residual anti-CD3 mAb bound at the cell surface, tCD3s were immunoprecitated with secondary antibodies and protein A-Sepharose (tCD3 IP) (see scheme in figure S6A). Immunoprecipitates from lysates of cells treated similarly without the addition of anti-CD3ε mAb were used as negative controls (neg ctr). Immunoprecipitates were probed with the indicated antibodies. The results from two representative experiments are shown (n=4). The quantifications of the relative intensities of the immunoreactive bands (KD vs ctr) are shown in the box. **D**. Immunoblot analysis of GFP-specific immunoprecipitates from post-nuclear supernatants of Jurkat cells transiently transfected with a plasmid construct encoding GFP-tagged CCDC28B (CCDC-GFP

IP). Immunoprecipitates carried out with non-immune Abs were used as negative control (neg ctr). **E,F**. Immunoblot analysis of WASH-specific (E) or VPS35-specific (F) immunoprecipitates from post-nuclear supernatants of control or CCDC28B KD Jurkat cells. Immunoprecipitates carried out with non-immune Abs were used as negative control (neg ctr). For each panel the quantifications of the relative intensities of the immunoreactive bands (KD vs ctr) are shown in the box (n=4). **G,H**. Immunoblot analysis of GSH-Sepharose pull-down assays on post-nuclear supernatants of Jurkat cells using either GST fusion proteins encoding the N-terminal (GST-FAMn) and C-terminal (GST-FAMc) portions of the L-F-[D/E](3-10)-L-F repeat-rich tail of FAM21 (G), or a GST fusion protein encoding a portion of WASH spanning the WDH1, WDH2 and PR domains (H) (see schemes in figure S6B). Recombinant GST was used as negative control. For each filter the Ponceau staining is shown (n=3). Total post-nuclear supernatants (lys) were included in all gels. The migration of molecular mass markers is shown for each filter. Error bars, SD. ***, $p<0.001$; **, $p<0.01$; *, $p<0.05$ (Student's t-test).

Figure 7. T cells from CVID patients heterozygous for the C211T *ccdc28b* allele display IS defects that can be rescued by overexpression of the wild-type allele. **A.** ^{3}H-thymidine incorporation in triplicate samples of PBMC purified from 4 healthy donors (HD), 5 CVID patients homozygous for wild-type *ccdc28b* (CVID wt) and 7 patients heterozygous for the C211T *ccdc28b* allele (CVID mut) and activated on plate-bound anti-CD3ε mAb (OKT3) for 72 h. Data are expressed as counts per minute (cpm). **B-D**. Immunofluorescence analysis of CD3ζ (B), tyrosine phosphoproteins (C) or γ-tubulin (D) in 15-min conjugates of HD, CVID-wt and CVID-mut T cells and Raji cells pulsed with a mix of SEA, SEB and SEE. For each panel the scattered dot plot

show, for each individual, the quantification (%) of conjugates with CD3ζ, PTyr or γ-tubulin staining at the IS (n conjugates =100) (B-D, left); for CD3ζ and PTyr the relative fluorescence at the T-cell:APC contact site compared to the remaining T-cell area (recruitment index) (B,C, right); for γ-tubulin the mean distance from the T-cell:APC contact site (μm) (n=25 conjugates) (D, right). **E**. Graphs showing, for each individual, the quantification (%) of conjugates with CD3ζ (left) or PTyr (right) accumulation at the IS in 15-min conjugates of HD, CVID-wt and CVID-mut T cells, nucleofected with either a GFP-encoding vector or the same vector encoding wild-type GFP-tagged CCDC28B and SEA/SEB/SEE-pulsed Raji cells (n conjugates =30). **F**. Immunofluorescence analysis of F-actin in 15 min-conjugates of HD, CVID-wt and CVID-mut T cells stained with fluorochrome-tagged phalloidin. The scattered dot plots show, for each individual, the quantification (%) of conjugates with F-actin staining at the IS (n conjugates =100) (left) or the relative fluorescence of F-actin at the T-cell:APC contact site compared to the remaining T-cell area (recruitment index) (n=25 conjugates) (right). **G-I**. Immunofluorescence analysis of recycling TCRs (tCD3; see legend to figure 4E for experimental setting) in HD, CVID-wt and CVID-mut T cells conjugated for 15 min with SEA/SEB/SEE-pulsed Raji cells and co-stained for F-actin (G), WASH (H) or FAM21 (I). For each panel the histograms show, for each individual, the co-localization of tCD3 with F-actin, WASH or FAM21 on individual dots (left, Mander's coefficient), or the quantification of $tCD3^+$ dots positive for the same markers (right, %). Measurements were taken on 50 conjugates and a mean of 10 dots per cell were analyzed. Error bars, SD. ****, p≤0.0001; ***, p≤0.001; **, p≤0.01; *, p≤0.05 (One-way analysis of variance (ANOVA), multiple comparisons).

Figure 8. The CCDC28B R25 residue mutated in CVID is required for coupling FAM21/WASH to the retromer complex. A. Immunoblot analysis with anti-CCDC28B antibodies of Jurkat cells transiently transfected with plasmids encoding GFP-tagged wild-type CCDC28B (wt) or GFP-tagged CCDC28B^{R25W} (mut). The recombinant and endogenous forms are indicated. Actin was used as loading control. **B-D**. Immunofluorescence analysis of CD3ζ (B), tyrosine phosphoproteins (C) or F-actin (D) in 15-min conjugates of Jurkat cells expressing GFP-tagged wild-type CCDC28B (wt) or GFP-tagged CCDC28B^{R25W} (mut) and SEE-pulsed Raji cells (APC). In each panel the histograms show the quantification (%) of conjugates with CD3ζ, PTyr or F-actin staining at the T cell:APC contact site (at least 100 conjugates were analyzed for each marker) (n≥3) (left) and the relative fluorescence of CD3ζ, PTyr or F-actin at the T-cell:APC contact site compared to the remaining T-cell area (recruitment index) (n=30 conjugates) (right). **E-G.** Immunofluorescence analysis of recycling TCRs (tCD3; see legend to figure 4E for experimental setting) in in 15-min conjugates of Jurkat cells expressing GFP-tagged wild-type CCDC28B (wt) or GFP-tagged CCDC28B^{R25W} (mut) and SEE-pulsed Raji cells (APC), co-stained for F-actin (E), WASH (F) or FAM21 (G). For each panel the histograms show the quantification of tCD3^{+} dots positive for F-actin, WASH or FAM21 (left, %); and the co-localization of tCD3 with F-actin, WASH or FAM21 on individual dots (bottom, Mander's coefficient). Measurements were taken on 50 conjugates from at least 3 independent experiments and a mean of 10 dots per cell were analyzed. **H**. Immunoblot analysis of GFP-specific immunoprecipitates (CCDC-GFP IP) from post-nuclear supernatants of Jurkat cells transiently transfected with plasmids encoding GFP-tagged wild-type CCDC28B (wt) or GFP-tagged CCDC28B^{R25W} (mut). Immunoprecipitates carried out with non-immune Abs were used as negative control (neg ctr). The quantifications of the relative

intensities of the immunoreactive bands (mut vs ctr) are shown in the box (n=5). **I**. Immunoblot analysis of GSH-Sepharose pull-down assays on post-nuclear supernatants of Jurkat cells using GST fusion proteins encoding wild-type CCDC28B (GST-wt), or CCDC28B^{R25W} (GST-mut), or the CCDC28B CC domain (GST-CC), or a CCDC28 deletion mutant lacking the CC domain (ΔCC) (see schemes in figure S6B). Recombinant GST was used as negative control. For each filter the Ponceau staining is shown (n=3). Total post-nuclear supernatants (lys) were included in all gels. The migration of molecular mass markers is shown for each filter. Error bars, SD. ***, $p<0.001$; **, $p<0.01$; *, $p<0.05$ (Student's t-test).

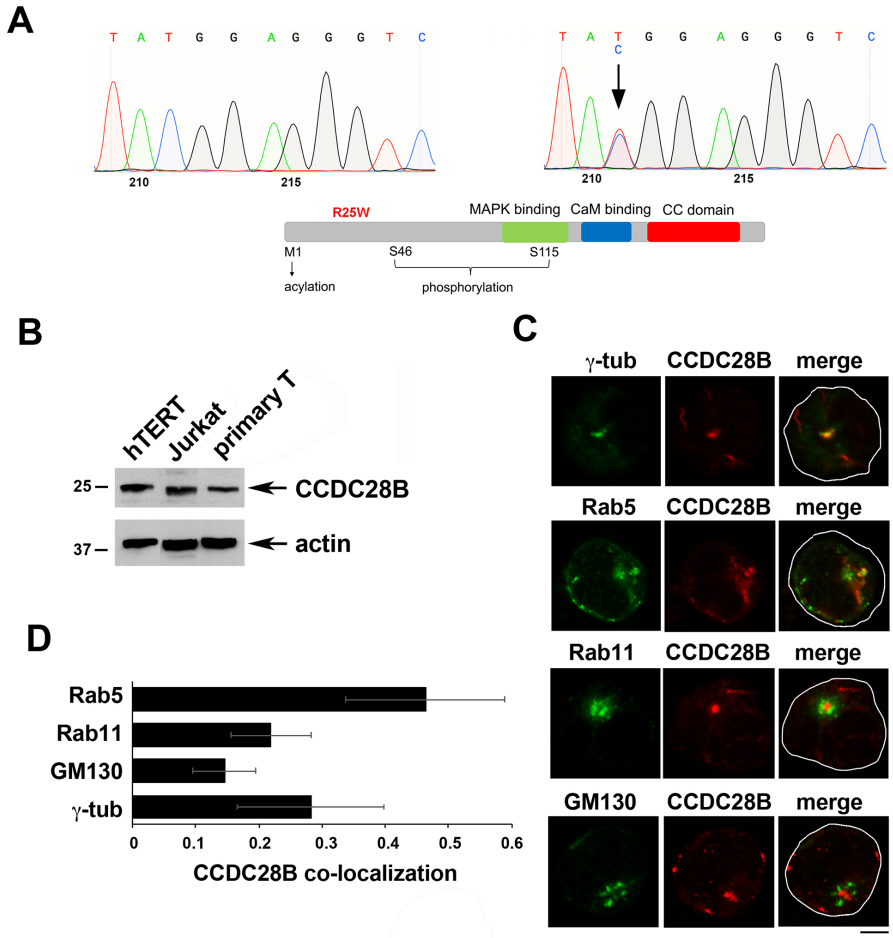
A
T A T G G A G G G T C
210
215
T A T C G G A G G G T C
210
215
R25W
MAPK binding
CaM binding
CC domain
M1
acylation
S46
S115
phosphorylation
B
hTERT
Jurkat
primary T
25
CCDC28B
37
actin
C
γ-tub
CCDC28B
merge
Rab5
CCDC28B
merge
Rab11
CCDC28B
merge
GM130
CCDC28B
merge
D
Rab5
Rab11
GM130
γ-tub
0
0.1
0.2
0.3
0.4
0.5
0.6
CCDC28B co-localization
E
γ-tub
CCDC28B
merge
DIC
APC
T
no SEE
+ SEE
F
γ-tub
CCDC28B
merge
DIC
APC
T
no SAg
+ SAg

FIGURE 1

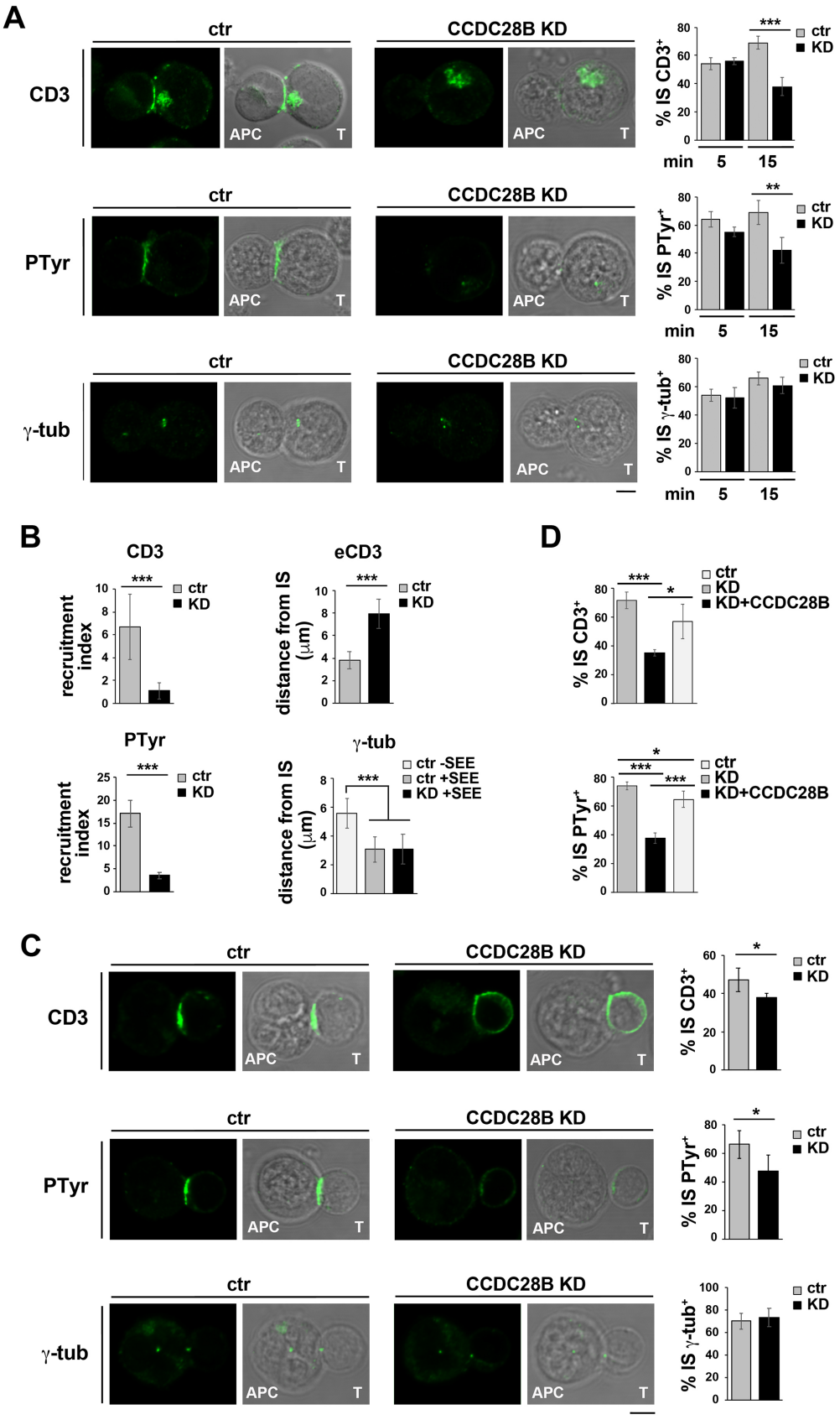
A
ctr
CCDC28B KD
CD3
PTyr
γ-tub
APC
T
% IS CD3+
% IS PTyr+
% IS γ-tub+
min 5 15
ctr
KD
B
CD3
eCD3
PTyr
γ-tub
recruitment index
distance from IS (μm)
ctr -SEE
ctr +SEE
KD +SEE
D
KD+CCDC28B
C

FIGURE 2

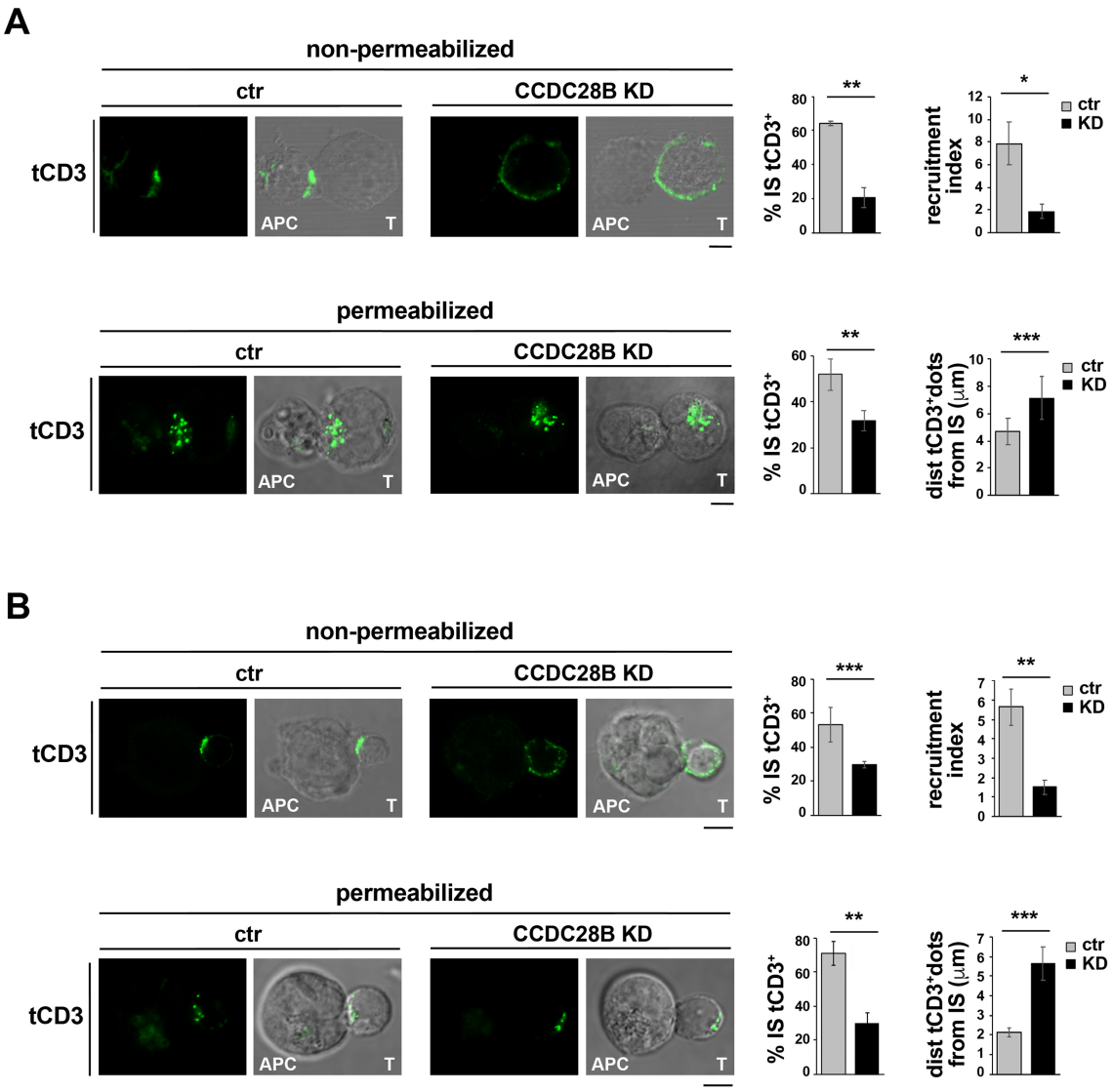
A
non-permeabilized
ctr
CCDC28B KD
tCD3
APC
T
% IS tCD3+
recruitment index
ctr
KD
permeabilized
dist tCD3+dots from IS (μm)
B

FIGURE 3

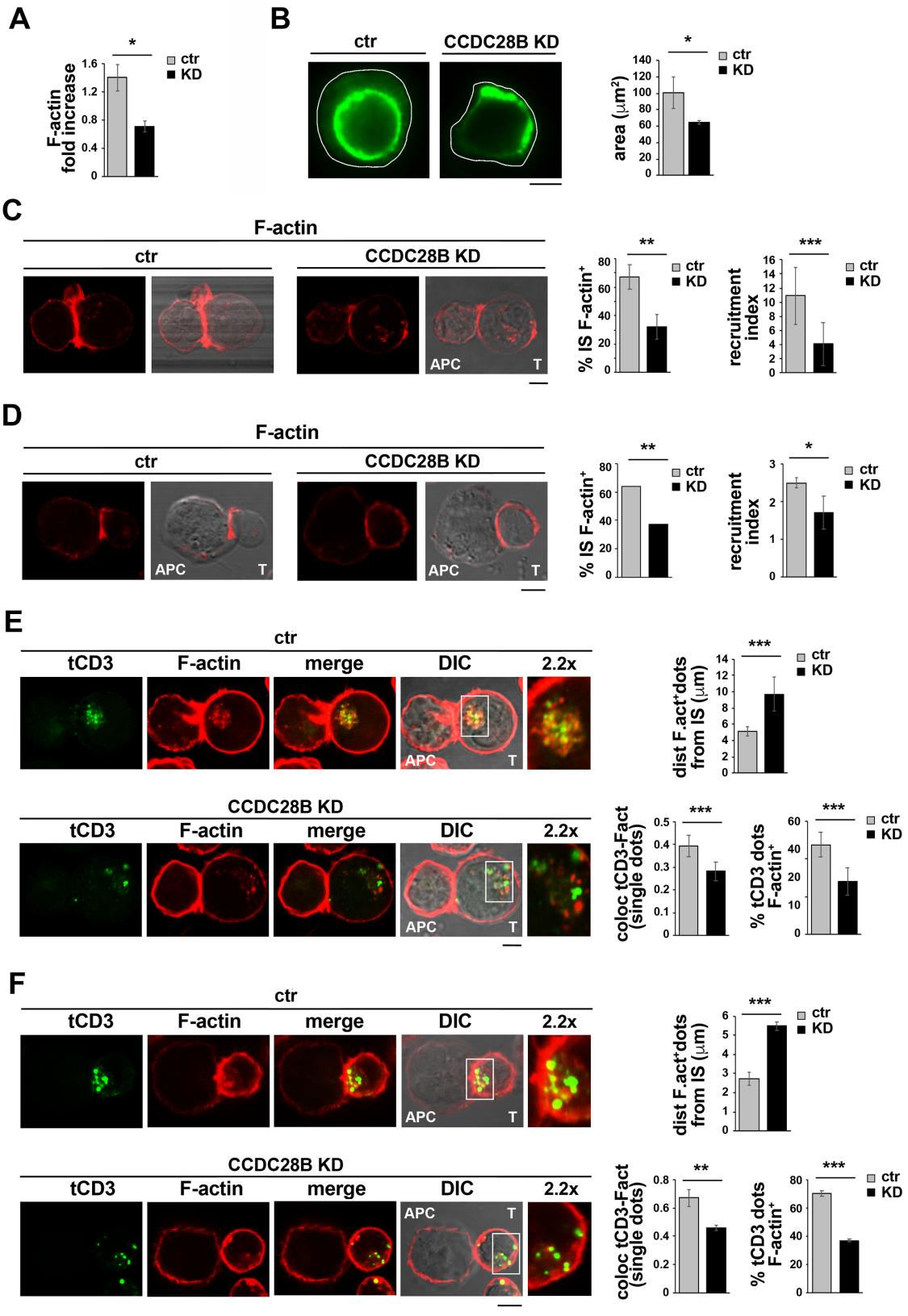
A
F-actin fold increase
ctr
KD
B
ctr
CCDC28B KD
area (μm²)
C
F-actin
ctr
CCDC28B KD
APC
T
% IS F-actin⁺
recruitment index
D
E
tCD3
F-actin
merge
DIC
2.2x
dist F.act⁺dots from IS (μm)
coloc tCD3-Fact (single dots)
% tCD3 dots F-actin⁺
F

FIGURE 4

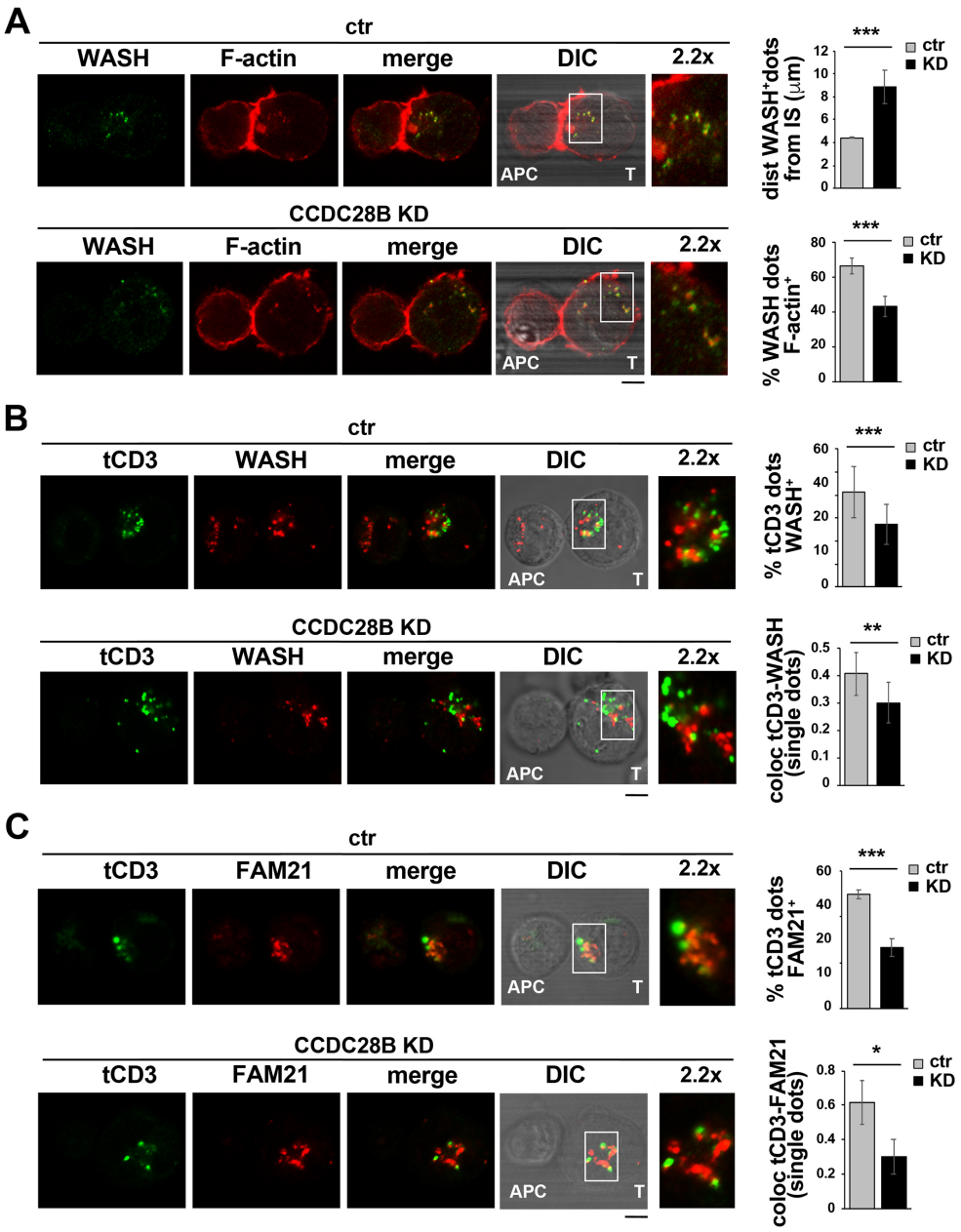
A
ctr
WASH
F-actin
merge
DIC
2.2x
APC
T
CCDC28B KD
dist WASH+dots from IS (μm)
% WASH dots F-actin+
***
ctr
KD
B
tCD3
WASH
% tCD3 dots WASH+
coloc tCD3-WASH (single dots)
**
C
FAM21
% tCD3 dots FAM21+
coloc tCD3-FAM21 (single dots)
*

FIGURE 5

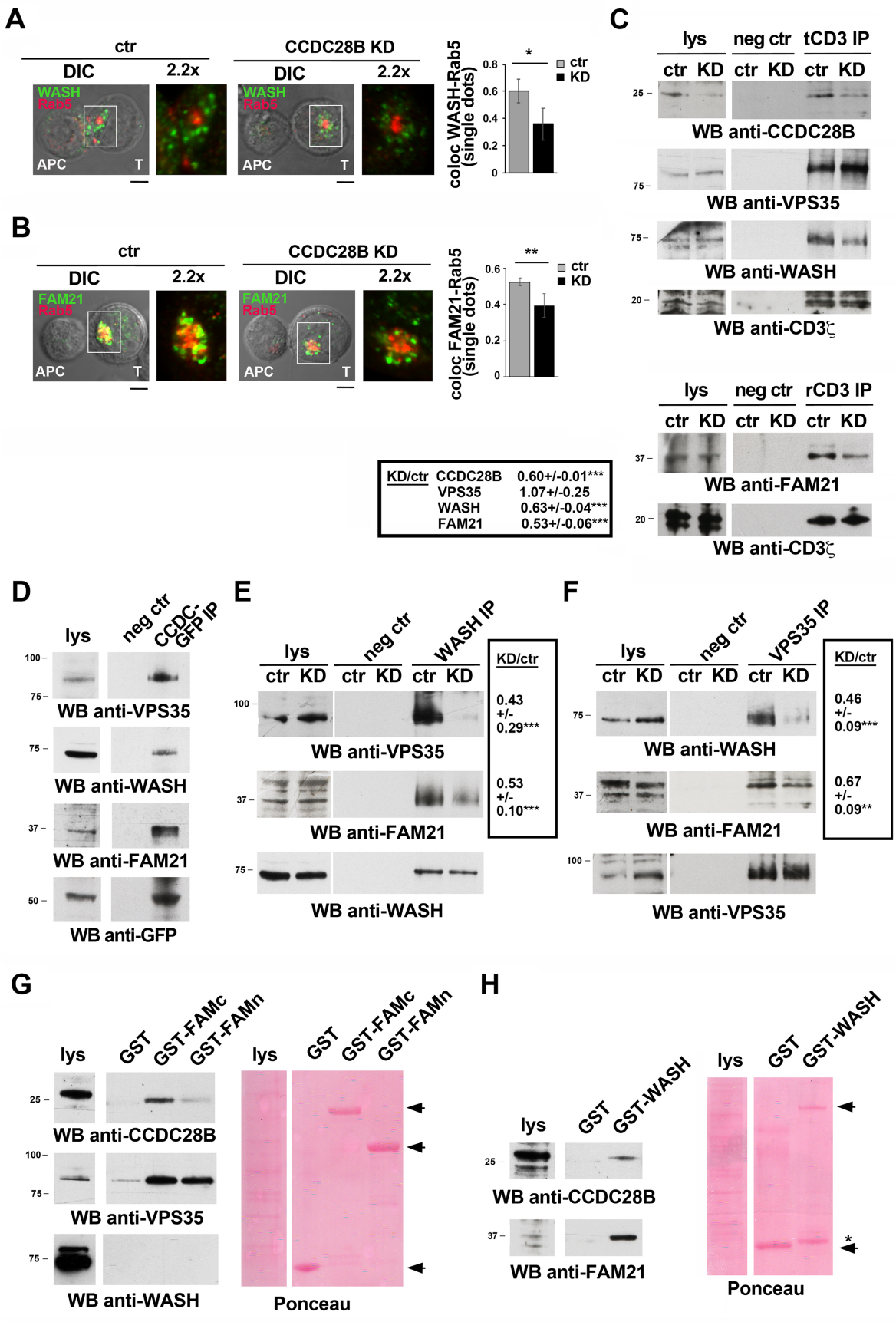
A
ctr
CCDC28B KD
DIC
2.2x
WASH
Rab5
APC
T
coloc WASH-Rab5 (single dots)
ctr
KD
B
FAM21
coloc FAM21-Rab5 (single dots)
C
lys
neg ctr
tCD3 IP
WB anti-CCDC28B
WB anti-VPS35
WB anti-WASH
WB anti-CD3ζ
rCD3 IP
WB anti-FAM21
KD/ctr
CCDC28B 0.60+/-0.01***
VPS35 1.07+/-0.25
WASH 0.63+/-0.04***
FAM21 0.53+/-0.06***
D
CCDC-GFP IP
WB anti-GFP
E
WASH IP
0.43 +/- 0.29***
0.53 +/- 0.10***
F
VPS35 IP
0.46 +/- 0.09***
0.67 +/- 0.09**
G
GST
GST-FAMc
GST-FAMn
Ponceau
H
GST-WASH

FIGURE 6

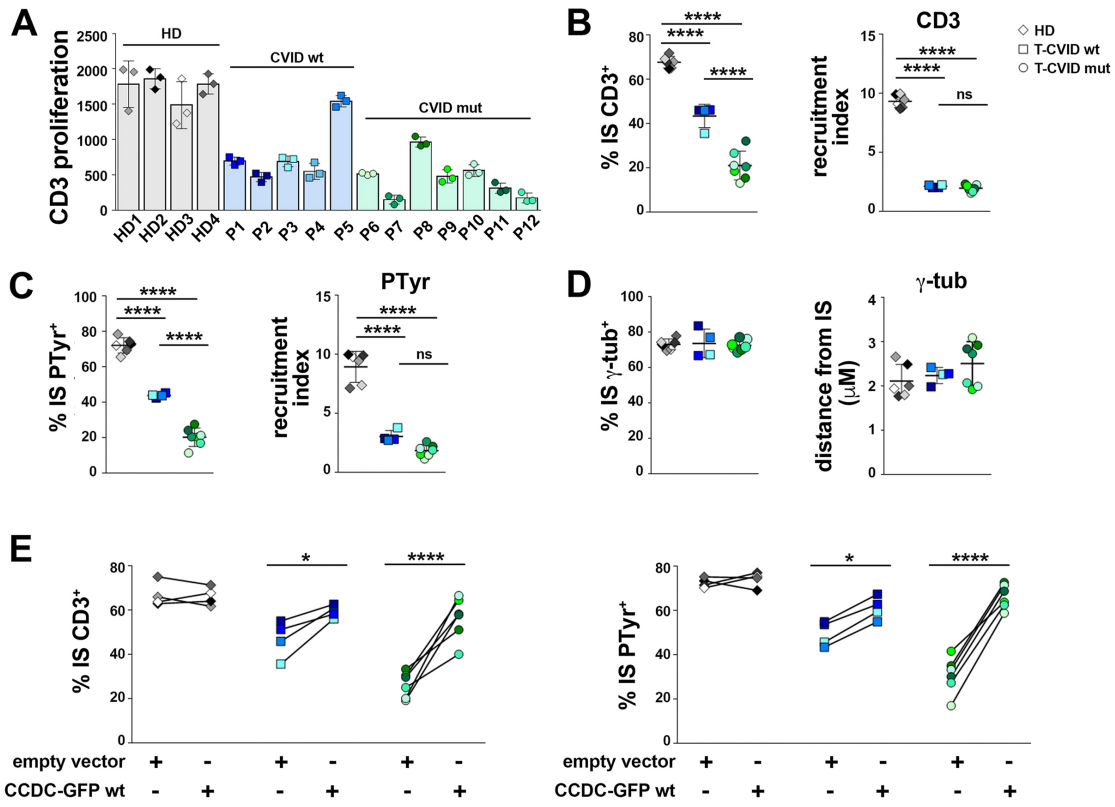
A
CD3 proliferation
HD
CVID wt
CVID mut
HD1 HD2 HD3 HD4 P1 P2 P3 P4 P5 P6 P7 P8 P9 P10 P11 P12
B
% IS CD3+
CD3
recruitment index
HD
T-CVID wt
T-CVID mut
C
% IS PTyr+
PTyr
recruitment index
D
% IS γ-tub+
γ-tub
distance from IS (μM)
E
% IS CD3+
% IS PTyr+
empty vector
CCDC-GFP wt
F
% IS F-actin+
act
recruitment index
G
coloc tCD3-Fact (single dots)
% tCD3 dots F-actin+
H
coloc tCD3-WASH (single dots)
% tCD3 dots WASH+
I
coloc tCD3-FAM21 (single dots)
% tCD3 dots FAM21+

FIGURE 7

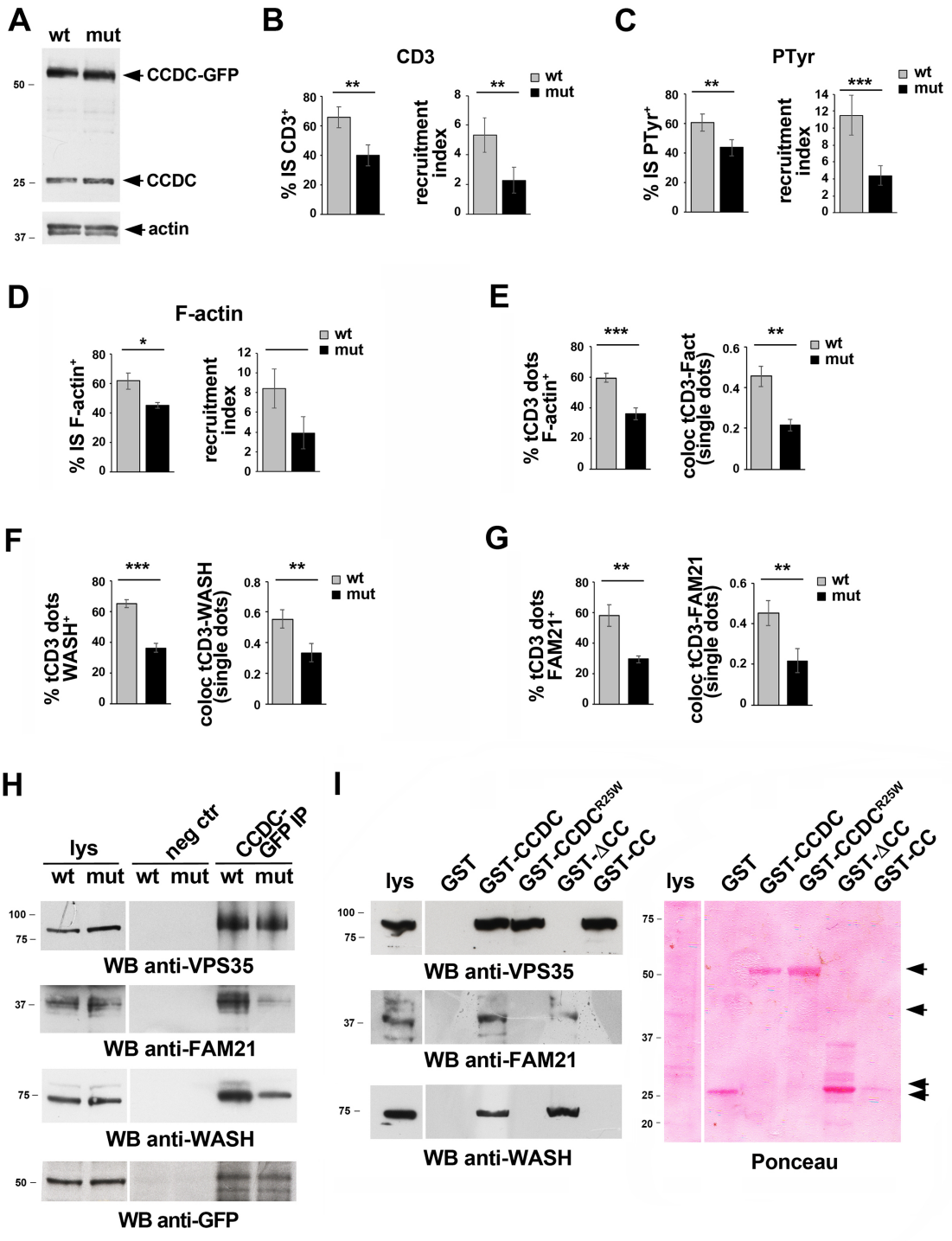
A
wt mut
50 –
25 –
37 –
CCDC-GFP
CCDC
actin
B
CD3
% IS CD3+
recruitment index
wt
mut
C
PTyr
% IS PTyr+
recruitment index
D
F-actin
% IS F-actin+
recruitment index
E
% tCD3 dots F-actin+
coloc tCD3-Fact (single dots)
F
% tCD3 dots WASH+
coloc tCD3-WASH (single dots)
G
% tCD3 dots FAM21+
coloc tCD3-FAM21 (single dots)
H
lys
neg ctr
CCDC-GFP IP
WB anti-VPS35
WB anti-FAM21
WB anti-WASH
WB anti-GFP
I
lys
GST
GST-CCDC
GST-CCDCR25W
GST-ΔCC
GST-CC
WB anti-VPS35
WB anti-FAM21
WB anti-WASH
Ponceau

FIGURE 8

Figures

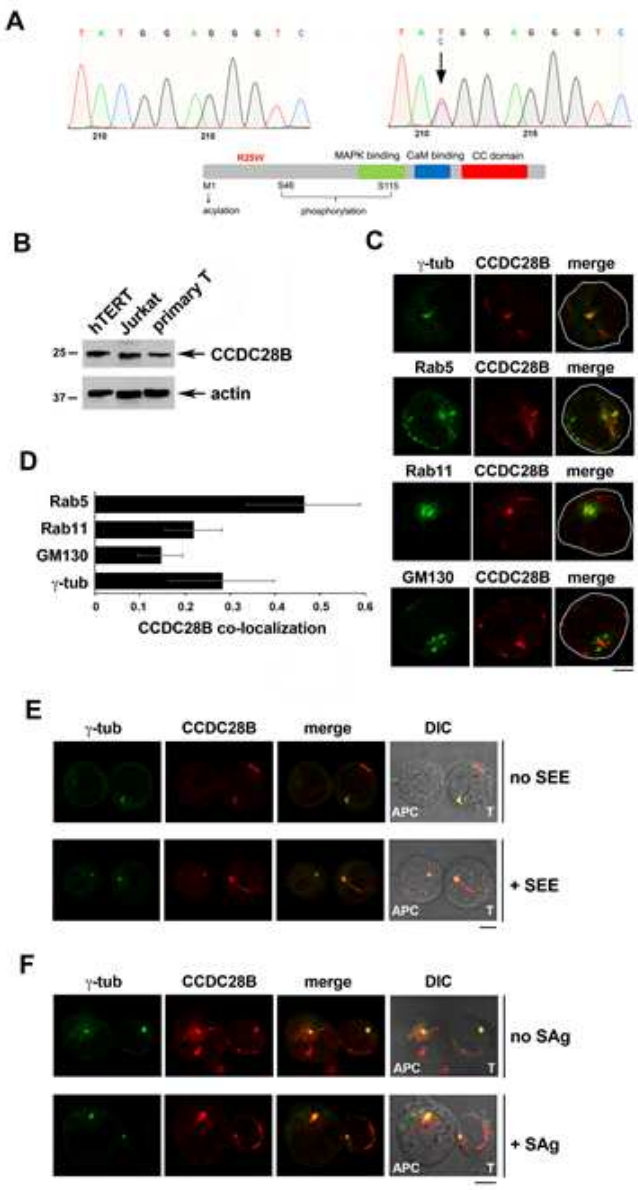

FIGURE 1

Figure 1

CCDC28B is expressed in T cells and is recruited to the IS. A. Sanger sequencing chromatograms of the PCR amplification products of ccdc28b (NG_012178.1, nucleotide positions 6289-6510, corresponding to cDNA nucleotide positions 116-302, covering the entire exon 2) on genomic DNA from representative

CVID patients carrying either the wild-type ccdc28b allele (left) or heterozygous for the C211T allele (right). A scheme of the domain organization of CCDC28B is shown below. B. Representative immunoblot of CCDC28B in lysates of hTERT-immortalized fibroblasts, Jurkat T cells and primary T cells. C,D. Immunofluorescence analysis and co-localization of CCDC28B and in Jurkat cells costained with antibodies to g-tubulin (centrosome), Rab5 (early endosome), Rab11 (recycling endosome) or GM130 (Golgi apparatus). Representative images (medial optical sections) are shown in C. The quantification (mean±SD) using Mander's coefficient of the weighted co-localization of CCDC28B with each marker is shown in D. 30 cells were analyzed for each marker (n=3). E,F. Immunofluorescence analysis of CCCDC28B and g-tubulin in conjugates of Jurkat cells and SEE-pulsed Raji cells (APC) (E), or primary T cells and Raji cells pulsed with a mix of SEA, SEB and SEE (SAg) (F). Conjugates formed in the absence of SEE/SAg were used as negative controls. Representative images (medial optical sections) are shown (n=3). Size bar, 5 μm.

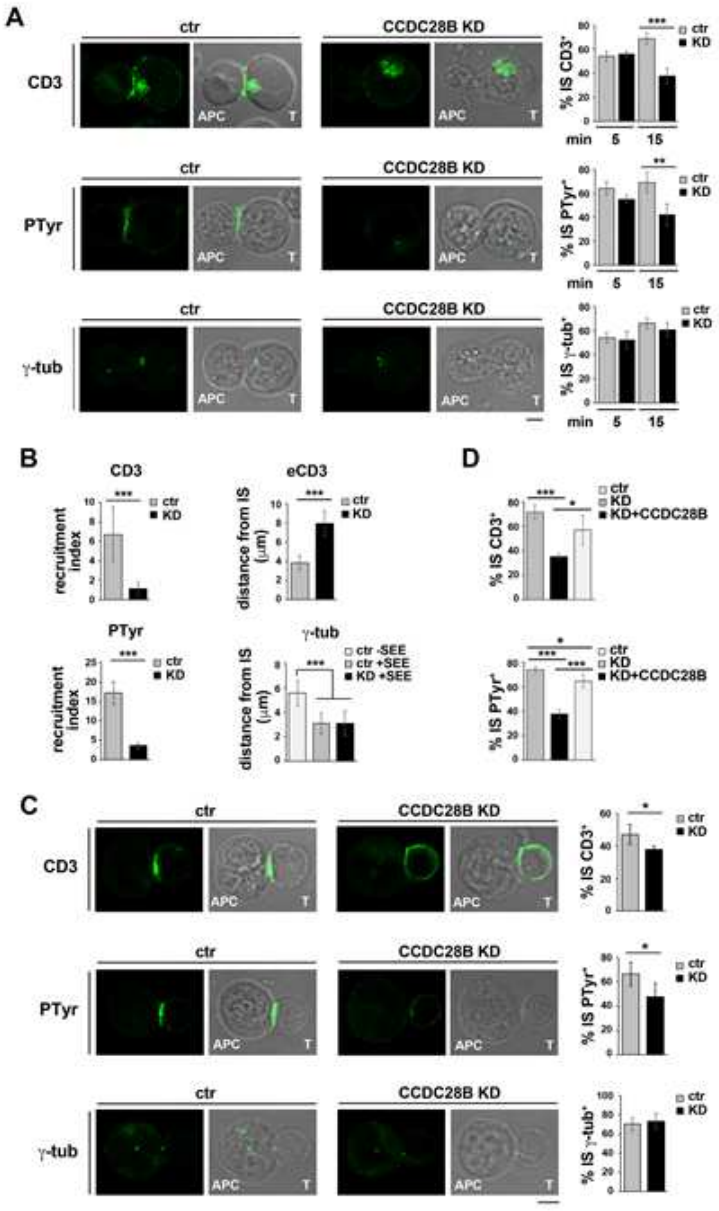

FIGURE 2

Figure 2

CCDC28B is required for immune synapse assembly. A. Immunofluorescence analysis of CD3z (top), tyrosine phosphoproteins (PTyr) (middle) or g-tubulin (bottom) in 15-min conjugates of control or CCDC28B KD Jurkat cells and SEE-pulsed Raji cells (APC). The histograms show the quantification (%) of conjugates with CD3z, PTyr or g-tubulin staining at the T cell:APC contact site 5 min and 15 min after conjugate formation. At least 100 conjugates were analyzed for each marker (n≥3). B. Left, Histograms

showing the relative fluorescence of CD3z (top; includes membrane and endosomal CD3z) or PTyr (bottom) at the T-cell:APC contact site compared to the remaining T-cell area (recruitment index). Right, histogram showing the mean distance of CD3z+ endosomes (eCD3, top) or of the centrosome (g-tub, bottom) from the T-cell:APC contact site (μm). Measurements were taken on 50 conjugates (n≥3). C. Immunofluorescence analysis of CD3z (top), tyrosine phosphoproteins (PTyr) (middle) or g-tubulin (bottom) in conjugates of control or CCDC28B KD primary T cells cells and Raji cells (APC) pulsed with a mix of SEA, SEB and SEE. The histograms show the quantification (%) of conjugates with CD3z, PTyr or g-tubulin staining at the IS 15 min after conjugate formation. At least 100 conjugates were analyzed for each marker (n≥3). D. Histograms showing the quantification (%) of 15-min conjugates with CD3z, PTyr or g-tubulin staining at the IS in conjugates of control or CCDC28B KD Jurkat cells, transfected with either empty vector (ctr, KD) or the same vector encoding wild-type CCDC28B (KD+CCDC28B), and SEE-pulsed Raji cells. At least 50 conjugates were analyzed for each marker (n≥3). Size bar, 5 μm. Error bars, SD. ***, $p<0.001$; **, $p<0.01$; *, $p<0.05$ (Student's ttest).

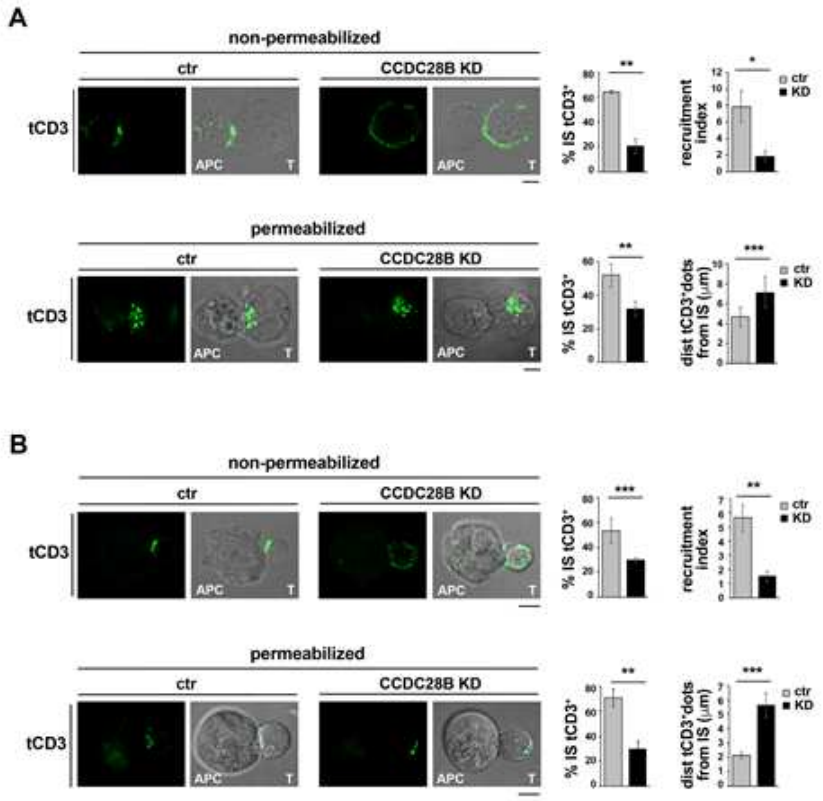

FIGURE 3

Figure 3

CCDC28B is required for polarized TCR recycling to the IS. A,B. Immunofluorescence analysis of recycling TCRs (tCD3) in control or CCDC28B KD Jurkat cells conjugated for 15 min with SEE-pulsed Raji cells (APC) (A) or primary T cells conjugated with SEA/SEB/SEE-pulsed Raji cells (B). Before conjugation, cells were added with anti-CD3e mAb (OKT3) and incubated at 37°C for 2 h to allow for internalization of CD3-Ab complexes. Following acid-stripping to remove residual anti- CD3 mAb bound at the cell surface.

Conjugates were stained with secondary fluorescently-labelled antibodies, after fixing either under non-permeabilizing conditions (top) or after cell permeabilization (bottom). The histograms show the quantification (%) of conjugates with tCD3 at the IS (left). The histograms on the right show either the relative fluorescence of tCD3 at the T-cell:APC contact site compared to the remaining T-cell area (recruitment index) for non-permeabilized conjugates, or the mean distance of tCD3+ endosomes from the T-cell:APC contact site (μm) for permeabilized conjugates. At least 20 conjugates were analyzed in each experiment (n≥3). Size bar, 5 μm. Error bars, SD. ***, p<0.001; **, p<0.01; *, p<0.05 (Student's ttest).

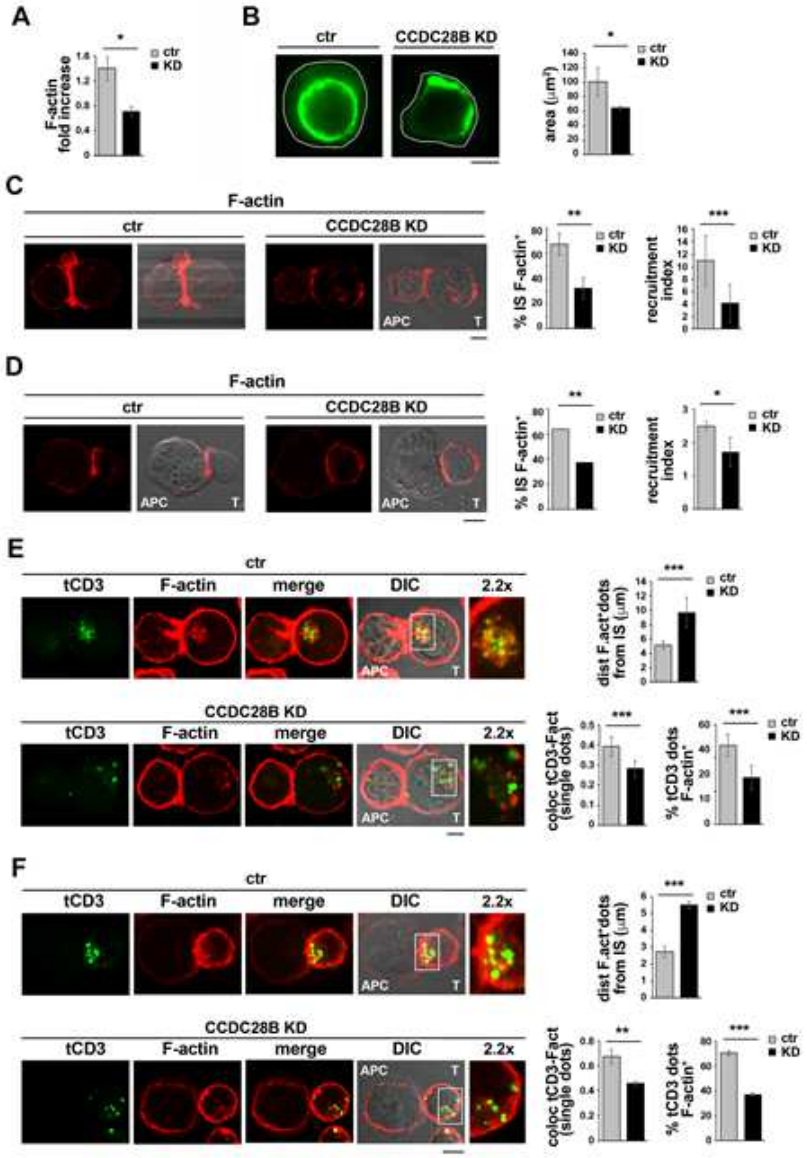

FIGURE 4

Figure 4

CCDC28B is required for TCR-dependent F-actin polymerization. A. Flow cytometric analysis of F-actin polymerization in response to TCR engagement in phalloidin-stained control or CCDC28B KD Jurkat cells. Cells were stimulated with soluble anti-CD3e mAb (UCHT-1) for 15 min. The data are expressed as fold increase of F-actin in stimulated vs non-stimulated cells (n=3). B. TIRF microscopy-based analysis of F-actin in phalloidin-stained control or CCDC28B KD Jurkat cells activated by plating on anti-CD3e mAb (UCHT-1)-coated coverslips for 15 min. The histogram shows the cell area (μm2) as a measure of cell spreading (n cells=20, n=3). C,D. Immunofluorescence analysis of F-actin in 15 min-conjugates of control or CCDC28B KD Jurkat cells and SEE-pulsed Raji cells (APC) (C), or control or CCDC28B KD primary T cells and SEA/SEB/SEE-pulsed Raji cells (D) stained with fluorochrometagged phalloidin. The histograms show the quantification (%) of conjugates with Factin staining at the IS (at least 100 conjugates were analyzed, n≥3) (left) or the relative fluorescence of F-actin at the T-cell:APC contact site compared to the remaining Tcell area (recruitment index) (n=25 conjugates). E,F. Immunofluorescence analysis of recycling TCRs (tCD3) and F-actin in control or CCDC28B KD Jurkat cells conjugated for 15 min with SEE-pulsed Raji cells (APC) (E) or primary T cells conjugated with SEA/SEB/SEE- pulsed Raji cells (F). Before conjugation, cells were added with anti- CD3e mAb (OKT3) and incubated at 37°C for 2 h to allow for internalization of CD3- Ab complexes. Following acid-stripping to remove residual anti-CD3 mAb bound at the cell surface. Conjugates were permealized/fixed and stained with secondary fluorescently-labelled antibodies and fluorochrome-labelled phalloidin. The histograms show the mean distance of F-actin+ dots from the T-cell:APC contact site (top, μm); the co-localization of tCD3 with F-actin on individual dots (bottom left, Mander's coefficient); and the quantification of tCD3+ dots positive for F-actin (bottom right). Measurements were taken on 50 conjugates from at least 3 independent experiments and a mean of 10 dots per cell were analyzed. Size bar, 5 μm. Error bars, SD. ***, $p<0.001$; **, $p<0.01$; *, $p<0.05$ (Student’s t-test).

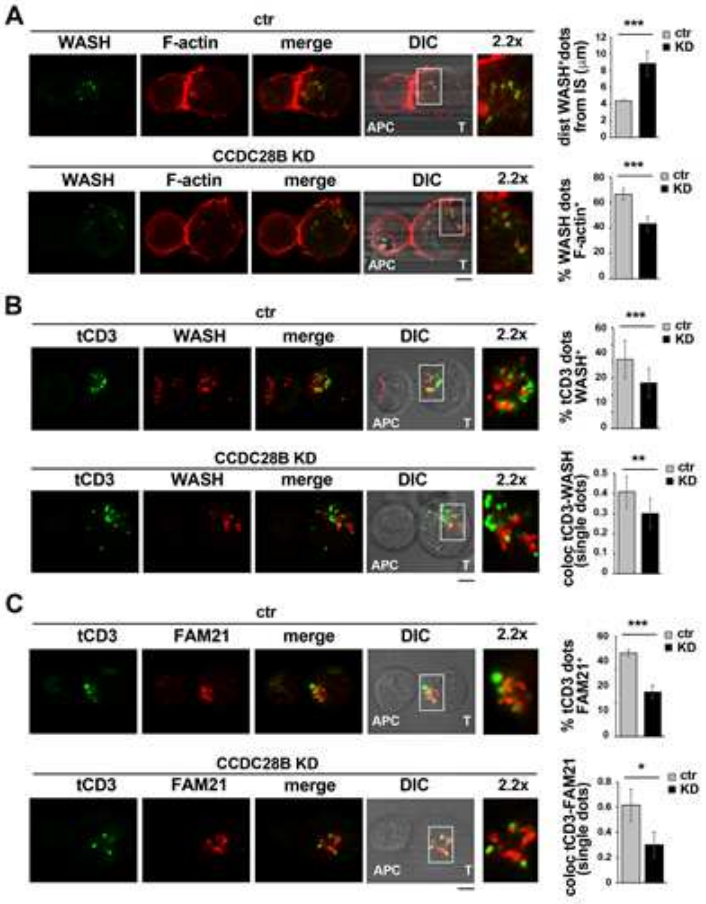

FIGURE 5

Figure 5

CCDC28B is required for recruitment of the actin regulator WASH and its adaptor FAM21 to recycling TCRs. A. Immunofluorescence analysis of WASH in 15 min-conjugates of control or CCDC28B KD Jurkat cells and SEE-pulsed Raji cells (APC) co-stained for F-actin. The histograms show the mean distance of WASH+ dots from the T-cell:APC contact site (top) and the quantification of WASH+ dots positive for actin (%, bottom). B,C. Immunofluorescence analysis of recycling TCRs (tCD3; see legend to figure 4E for

experimental setting) in control or CCDC28B KD Jurkat cells conjugated for 15 min with SEE-pulsed Raji cells (APC) and co-stained for WASH (B) or FAM21 (C). For each panel the histograms show the quantification of tCD3+ dots positive for WASH or FAM21 (top, %); and the co-localization of tCD3 with WASH or FAM21 on individual dots (bottom, Mander's coefficient). Measurements were taken on 50 conjugates from at least 3 independent experiments and a mean of 10 dots per cell were analyzed. Size bar, 5 µm. Error bars, SD. ***, p<0.001; **, p<0.01; *, p<0.05 (Student's t-test).

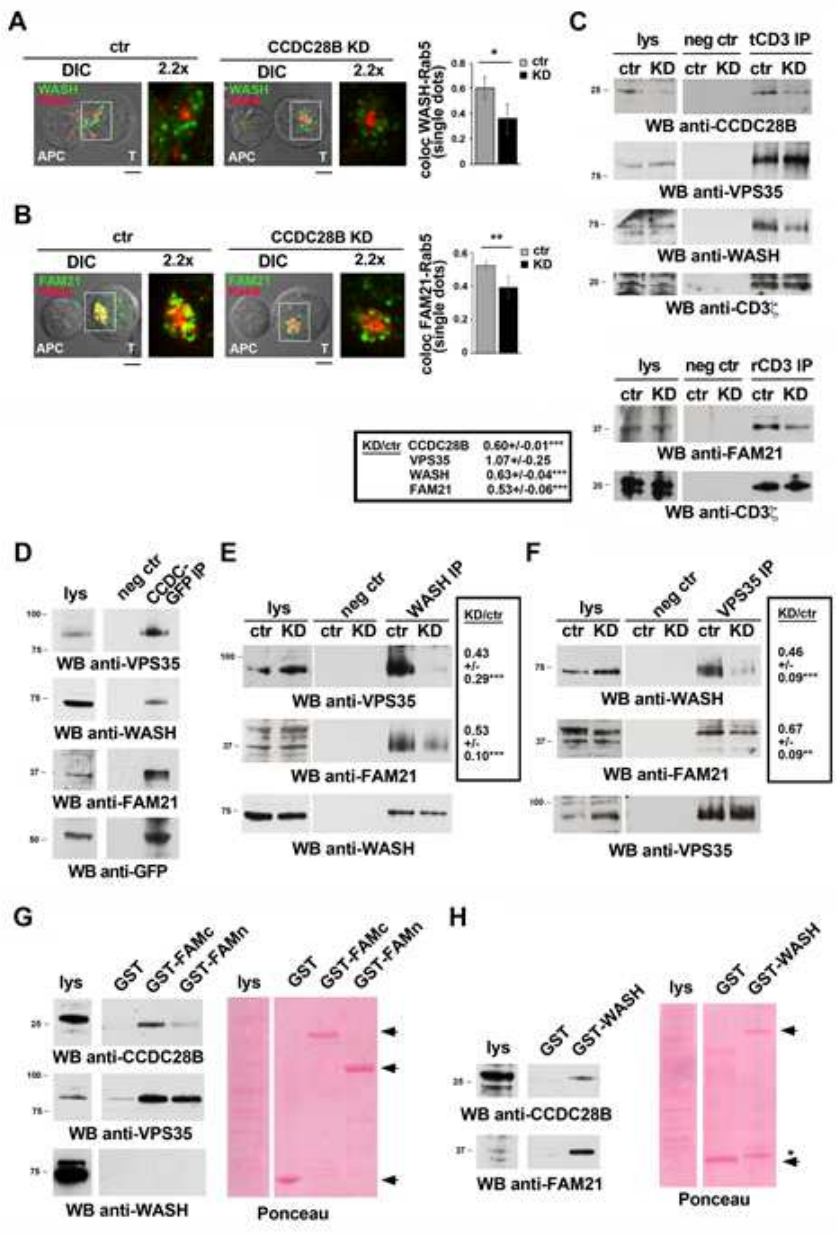

FIGURE 6

Figure 6

CCDC28B associates with recycling TCRs and forms a complex with WASH, FAM21 and VPS35. A-C. Immunofluorescence analysis of WASH (A) and FAM21 (B) in 15 min-conjugates of control or CCDC28B KD Jurkat cells and SEEpulsed Raji cells (APC) co-stained for Rab5. The histograms show the co-localization of WASH or FAM21 with Rab5 on individual dots (Mander's coefficient). Measurements were taken on 50 conjugates from at least 3 independent experiments and a mean of 10 dots per cell were analyzed. C. Immunoblot analysis of tCD3-specific immunoprecipitates from post-nuclear supernatants of control or CCDC28B KD Jurkat cells. Cells were added with anti-CD3e mAb (OKT3) and incubated at 37°C for 2 h to allow for internalization of CD3-Ab complexes. Following acid-stripping to remove residual anti-CD3 mAb bound at the cell surface, tCD3s were immunoprecitated with secondary antibodies and protein A-Sepharose (tCD3 IP) (see scheme in figure S6A). Immunoprecipitates from lysates of cells treated similarly without the addition of anti- CD3e mAb were used as negative controls (neg ctr). Immunoprecipitates were probed with the indicated antibodies. The results from two representative experiments are shown (n=4). The quantifications of the relative intensities of the immunoreactive bands (KD vs ctr) are shown in the box. D. Immunoblot analysis of GFP-specific immunoprecipitates from post-nuclear supernatants of Jurkat cells transiently transfected with a plasmid construct encoding GFP-tagged CCDC28B (CCDC-GFP IP). Immunoprecipitates carried out with non-immune Abs were used as negative control (neg ctr). E,F. Immunoblot analysis of WASH-specific (E) or VPS35-specific (F) immunoprecipitates from post-nuclear supernatants of control or CCDC28B KD Jurkat cells. Immunoprecipitates carried out with non-immune Abs were used as negative control (neg ctr). For each panel the quantifications of the relative intensities of the immunoreactive bands (KD vs ctr) are shown in the box (n=4). G,H. Immunoblot analysis of GSH-Sepharose pull-down assays on post-nuclear supernatants of Jurkat cells using either GST fusion proteins encoding the N-terminal (GST-FAMn) and Cterminal (GST-FAMc) portions of the L-F-[D/E](3-10)-L-F repeat-rich tail of FAM21 (G), or a GST fusion protein encoding a portion of WASH spanning the WDH1, WDH2 and PR domains (H) (see schemes in figure S6B). Recombinant GST was used as negative control. For each filter the Ponceau staining is shown (n=3). Total postnuclear supernatants (lys) were included in all gels. The migration of molecular mass markers is shown for each filter. Error bars, SD. ***, $p<0.001$; **, $p<0.01$; *, $p<0.05$ (Student’s t-test).

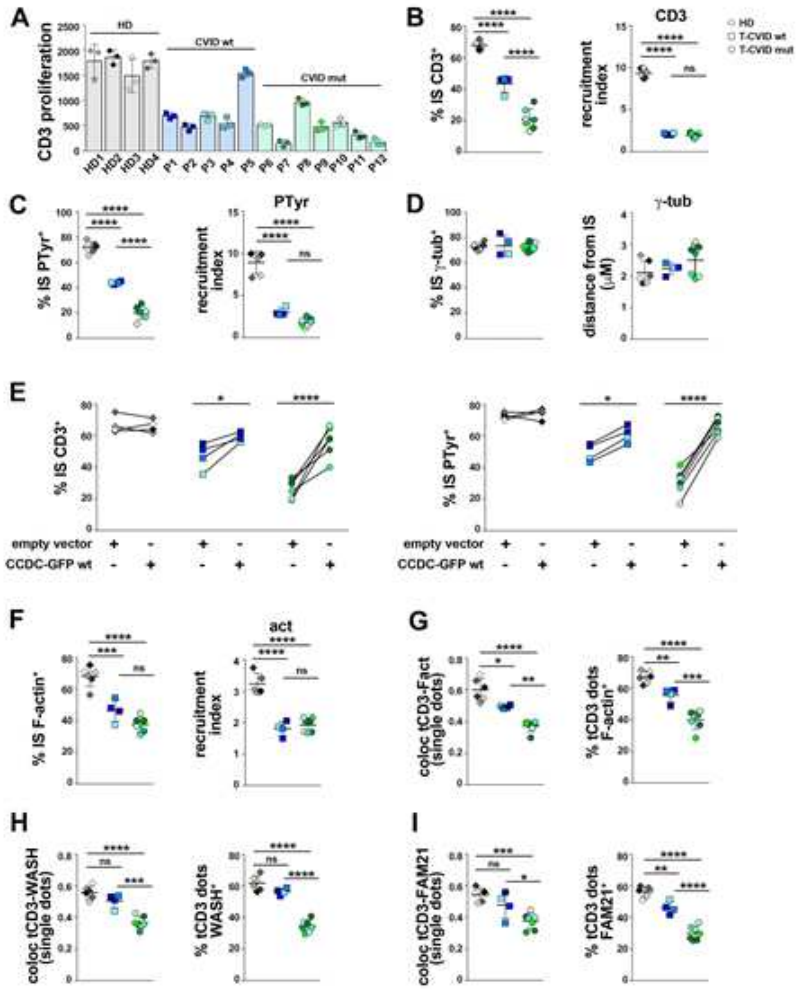

FIGURE 7

Figure 7

T cells from CVID patients heterozygous for the C211T ccdc28b allele display IS defects that can be rescued by overexpression of the wild-type allele. A. 3H-thymidine incorporation in triplicate samples of PBMC purified from 4 healthy donors (HD), 5 CVID patients homozygous for wild-type ccdc28b (CVID wt) and 7 patients heterozygous for the C211T ccdc28b allele (CVID mut) and activated on plate-bound anti-CD3e mAb (OKT3) for 72 h. Data are expressed as counts per minute (cpm). B-D. Immunofluorescence

analysis of CD3z (B), tyrosine phosphoproteins (C) or g-tubulin (D) in 15-min conjugates of HD, CVID-wt and CVID-mut T cells and Raji cells pulsed with a mix of SEA, SEB and SEE. For each panel the scattered dot plot show, for each individual, the quantification (%) of conjugates with CD3z, PTyr or gtubulin staining at the IS (n conjugates =100) (B-D, left); for CD3z and PTyr the relative fluorescence at the T-cell:APC contact site compared to the remaining T-cell area (recruitment index) (B,C, right); for g-tubulin the mean distance from the T-cell:APC contact site (μm) (n=25 conjugates) (D, right). E. Graphs showing, for each individual, the quantification (%) of conjugates with CD3z (left) or PTyr (right) accumulation at the IS in 15-min conjugates of HD, CVID-wt and CVID-mut T cells, nucleofected with either a GFP-encoding vector or the same vector encoding wild-type GFP-tagged CCDC28B and SEA/SEB/SEE-pulsed Raji cells (n conjugates =30). F. Immunofluorescence analysis of F-actin in 15 min-conjugates of HD, CVID-wt and CVID-mut T cells stained with fluorochrome-tagged phalloidin. The scattered dot plots show, for each individual, the quantification (%) of conjugates with F-actin staining at the IS (n conjugates =100) (left) or the relative fluorescence of F-actin at the T-cell:APC contact site compared to the remaining T-cell area (recruitment index) (n=25 conjugates) (right). G-I. Immunofluorescence analysis of recycling TCRs (tCD3; see legend to figure 4E for experimental setting) in HD, CVID-wt and CVID-mut T cells conjugated for 15 min with SEA/SEB/SEE-pulsed Raji cells and co-stained for F-actin (G), WASH (H) or FAM21 (I). For each panel the histograms show, for each individual, the co-localization of tCD3 with F-actin, WASH or FAM21 on individual dots (left, Mander's coefficient), or the quantification of tCD3+ dots positive for the same markers (right, %). Measurements were taken on 50 conjugates and a mean of 10 dots per cell were analyzed. Error bars, SD. ****, $p \leq 0.0001$; ***, $p \leq 0.001$; **, $p \leq 0.01$; *, $p \leq 0.05$ (One-way analysis of variance (ANOVA), multiple comparisons).

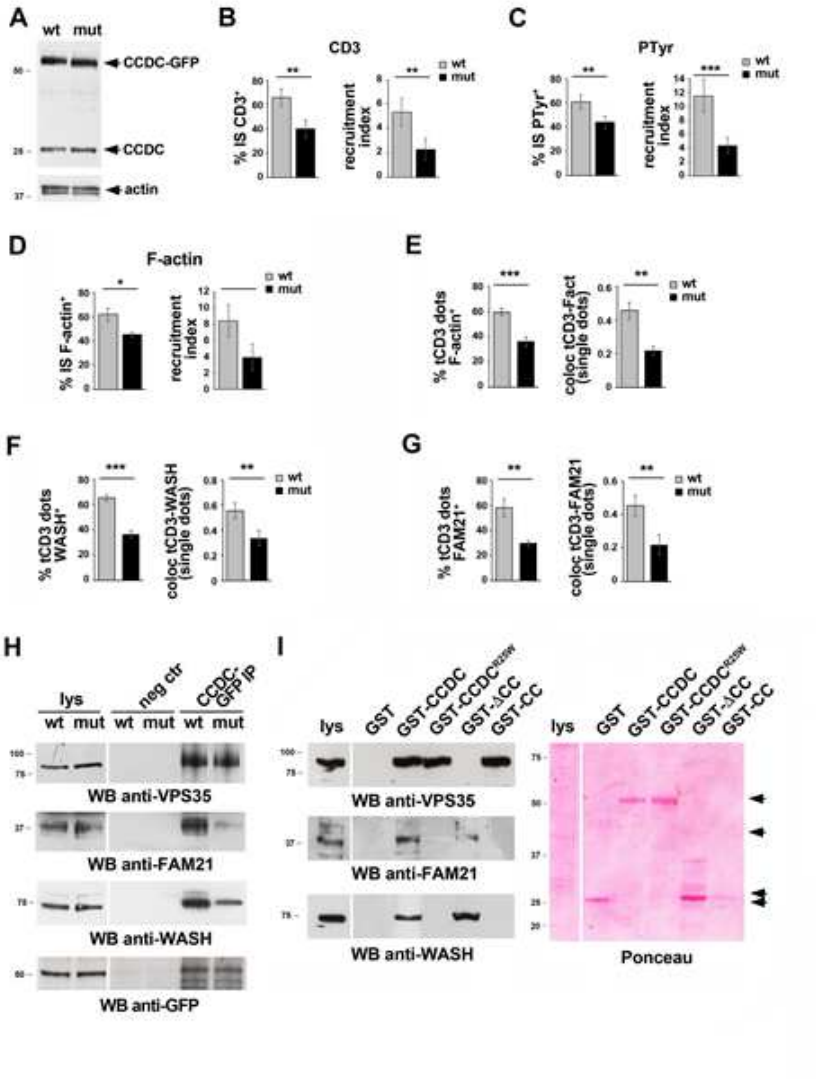

FIGURE 8

Figure 8

The CCDC28B R25 residue mutated in CVID is required for coupling FAM21/WASH to the retromer complex. A. Immunoblot analysis with anti-CCDC28B antibodies of Jurkat cells transiently transfected with plasmids encoding GFP-tagged wild-type CCDC28B (wt) or GFP-tagged CCDC28BR25W (mut). The recombinant and endogenous forms are indicated. Actin was used as loading control. B-D. Immunofluorescence analysis of CD3z (B), tyrosine phosphoproteins (C) or F-actin (D) in 15-min

conjugates of Jurkat cells expressing GFP-tagged wild-type CCDC28B (wt) or GFP-tagged CCDC28BR25W (mut) and SEE-pulsed Raji cells (APC). In each panel the histograms show the quantification (%) of conjugates with CD3z, PTyr or Factin staining at the T cell:APC contact site (at least 100 conjugates were analyzed for each marker) (n≥3) (left) and the relative fluorescence of CD3z, PTyr or F-actin at the T-cell:APC contact site compared to the remaining T-cell area (recruitment index) (n=30 conjugates) (right). E-G. Immunofluorescence analysis of recycling TCRs (tCD3; see legend to figure 4E for experimental setting) in in 15-min conjugates of Jurkat cells expressing GFP-tagged wild-type CCDC28B (wt) or GFP-tagged CCDC28BR25W (mut) and SEE-pulsed Raji cells (APC), co-stained for F-actin (E), WASH (F) or FAM21 (G). For each panel the histograms show the quantification of tCD3+ dots positive for F-actin, WASH or FAM21 (left, %); and the co-localization of tCD3 with F-actin, WASH or FAM21 on individual dots (bottom, Mander's coefficient). Measurements were taken on 50 conjugates from at least 3 independent experiments and a mean of 10 dots per cell were analyzed. H. Immunoblot analysis of GFP-specific immunoprecipitates (CCDC-GFP IP) from post-nuclear supernatants of Jurkat cells transiently transfected with plasmids encoding GFP-tagged wild-type CCDC28B (wt) or GFP-tagged CCDC28BR25W (mut). Immunoprecipitates carried out with nonimmune Abs were used as negative control (neg ctr). The quantifications of the relative intensities of the immunoreactive bands (mut vs ctr) are shown in the box (n=5). I. Immunoblot analysis of GSH-Sepharose pull-down assays on post-nuclear supernatants of Jurkat cells using GST fusion proteins encoding wild-type CCDC28B (GST-wt), or CCDC28BR25W (GST-mut), or the CCDC28B CC domain (GST-CC), or a CCDC28 deletion mutant lacking the CC domain (DCC) (see schemes in figure S6B). Recombinant GST was used as negative control. For each filter the Ponceau staining is shown (n=3). Total post-nuclear supernatants (lys) were included in all gels. The migration of molecular mass markers is shown for each filter. Error bars, SD. ***, $p<0.001$; **, $p<0.01$; *, $p<0.05$ (Student’s t-test).

Supplementary Files

This is a list of supplementary files associated with this preprint. Click to download.

- SupplementalMaterial.pdf